# Debonding of External CFRP Plates from RC Structures Caused by Cyclic Loading Effects

By

Adriaan Jakobus Badenhorst

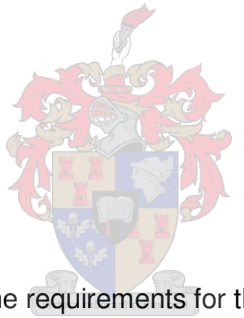

Thesis presented in fulfilment of the requirements for the degree of Master of Science in Engineering in the Faculty of Engineering at Stellenbosch University.

Supervisor: Professor GPAG van Zijl

March 2012

## Declaration

By submitting this thesis electronically, I declare that the entirety of the work contained therein is my own, original work, that I am the sole author thereof (save to the extent explicitly otherwise stated), that reproduction and publication thereof by Stellenbosch University will not infringe any third party rights and that I have not previously in its entirety or in part submitted it for obtaining any qualification.

Signed: .....

Date: .....

## Synopsis

This study set out to determine the debonding of externally applied Carbon Fibre Reinforced Polymer (CFRP) plates from RC structures under cyclic loading. Triplet shear tests and finite element (FE) analyses were done on the epoxy to determine the bond stress between the CFRP plate and a reinforced concrete specimen. From these tests and analyses the average shear strength of the bond between the epoxy and concrete substrate was determined and the shear strength of the epoxy specified by the supplier could be confirmed. A case study of a statically loaded beam was performed to verify the bond strength.

Finally a reinforced concrete (RC) T-section was designed and pre-cracked to simulate a damaged beam in practice. These sections were then externally reinforced by bonding CFRP plates onto the face of the web. The sections were subjected to static and cyclic loading at different force amplitudes. Along with the experimental tests, FE models were developed and analysed which had the same geometrical and material properties as the experimental specimens. Due to time constraint a FE mesh objectivity study was not done, but the chosen element size is believed to be sufficiently small to replicate the experimental tests objectively.

The FE analyses and the experimental tests yielded results that were close to each other on both the global scale and in terms of localised behaviour, thus it was decided that the computational approach could be used for the final design of a model of the debonding of CFRP plates bonded onto RC beams under cyclic loading because the data can be analysed more easily and a large variation of tests can be done.

For the T-section 3 tests were conducted; a pull-off (static) test where the bonded CFRP plate was pulled from a specimen to get the ultimate failure envelope of the test specimens. The static test was followed by cyclic tests with force amplitude of 85% and 65% of the ultimate pull-off strength. Different measurements were taken to get the global and local displacement behaviour of the section. The global displacement was measured by means of a linear variable displacement transducer (LVDT, displacement meter) clamped onto the CFRP plate that pushed on the top of the concrete and the local displacement was measured with the help of the Aramis system. The displacement was then compared to the same displacements of nodes and elements in the FE models. The result was a confirmation that the results from the FE models were sufficient to design a model for cyclic debonding of CFRP plates from RC structures.

From the FE models the relative displacement between the CFRP plate and concrete was obtained in the vicinity of a crack. This relative displacement was then normalised by the respective stress range of the different tests, from which the normalised relative displacement was plotted against the number of cycles to get an equation limiting the number of cycles for a specific stress range.

From the results, it appears that for cyclic load levels up to 65% of the peak static resistance, a threshold number of load cycles are required for delamination initiation. Subsequently, a near constant delamination rate is reached. The delamination rate is significantly lower for lower cyclic load levels. Finally, an unstable delamination stage is reached at a level of about 65 μm for all the analyses, after which CFRP pull-off is imminent.

Service life design of CFRP reinforcement of RC beams should take into consideration the delamination initiation threshold, the subsequent delamination rate and finally the initiation of unstable delamination.

## Opsomming

Die projek is uitgevoer om die delaminasie van ekstern aangewende Koolstof Vesel Versterkte Polimeer (KVVP) stroke op gewapende beton strukture te bepaal onder sikliese belasting. Triplet skuif toetse is gedoen op die gebruikte epoksie om die verband-sterkte te bepaaltussen die KVVP stroke en die beton proefstuk. Die skuif toetse is ook met behulp van die eindige element (EE) metode geanaliseer. Die resultaat van die toetse en analises het gewys dat die verband sterkte tussen die KVVP stroke en beton gelyk is aan die skuif sterkte van die epoksie wat verskaf is. `n Gevalle studie van `n monotonies belaste balk is gedoen om die verband-sterkte te verifieër.

`n Gewapende beton T-snit is ontwerp en voor-af gekraak om `n beskadigde balk in die praktyk voor te stel. Die beskadigde proefstukke is vervolgens ekstern versterk met KVVP stroke wat aan die web van die T-snit vas geplak is. Die versterkte T-snitte is getoets onder statiese en sikliese belasting. Die sikliese toetse is ook onder verskillende spanningsamplitudes getoets. Om die eksperimentele toetse te verifieër is EE modelle gebou en geanaliseer wat dieselfde geometriese en materiaal eienskappe as die eksperimentele proefstukke gehad het, maar as gevolg van `n tydsbeperking is `n sensitiwiteit studie oor die element grootte nie gedoen nie. Die element grootte is klein genoeg gekies en word beskou as voldoende om die gedrag objektief te simuleer.

Die EE analises en eksperimentele resultate was na genoeg aan mekaar op beide globale en lokale vlak. Dus is `n analitiese benadering tot die toetse vervolgens gebruik vir die ontwerp van `n model vir delaminasie van KVVP stroke van gewapende beton strukture onder sikliese belasting. Die EE metode stel die analis in staat om `n verskeidenheid van toetse relatief vinnig uit te voer en om die data van die toetse vinniger te interpreteer as deur fisiese eksperimentele toetse.

Drie eksperimente is uitgevoer op die T-snitte, `n aftrek-toets (staties) waar die KVVP strook van `n proefstuk afgetrek is om die falingsomhullende diagram te kry en dan ook twee sikliese toetse teen 85% en 65% van die krag amplitude van die falingskrag. Verplasingsmeters is gebruik om die globale verplasing te kry, deur dit vas te klamp op die KVVP strook en dan die verplasing te meet relatief tot die bokant van die beton. Die lokale veplasing is met behulp van die Aramis sisteem verkry. Die eksperimentele verplasings is dan vergelyk met verplasings van die ooreenstemmende nodes en elemente in die EE modelle. Deur die vergelyking van die resultate is dit bevestig dat die eindige element

modelle voldoende is om die model vir sikliese delaminasie van KVVP stroke van gewapende beton strukture te gebruik vir die ontwerp.

Uit die EE modelle is die relatiewe verplasing tussen die KVVP strook en die beton gekry in die omgewing van `n kraak. Die relatiewe verplasing is genormaliseer deur elkeen se spanningsamplitude. Die genormaliseerde relatiewe verplasing is dan teenoor die aantal siklusse geteken waarvan `n vergelyking vir die maksimum verplasing afgelei is om die aantal siklusse vir `n gegewe spanning amplitude te beperk.

Uit die resultate blyk dit dat vir sikliese laste tot en met 65% van die piek statiese weerstand `n aantal siklusse moontlik is voordat delaminasie begin waarna `n konstante delaminasie tempo bereik word. Die delaminasie tempo is stadiger vir sikliese laste teen `n laer belastings amplitude. Laastens word `n onstabiele delaminasie fase bereik by `n vlak van ongeveer 65 µm, na die oorgang delamineer die KVVP strook binne enkele siklusse.

Die beginpunt van delaminasie, die delaminasie tempo en laastens die begin van onstabiele delaminasie moet in gedagte gehou word by die ontwerp diens leeftyd van KVVP versterkte gewapende beton balke.

## Acknowledgements

I want to thank Professor GPAG van Zijl, my study leader, for giving me the opportunity to be his student and his guidance, support and advice he gave me during the conceptual design and execution of the work that was done during this project.

A great thank you to Stellenbosch University`s department of civil engineering and particular the structures division who gave me the opportunity to conduct the tests and make full use of their facilities.

Thank you Mapei South Africa (Pty) Ltd who sponsored the CFRP plates and epoxy for the experimental tests.

The lab assistants, Charlton Ramat and Reeza Ras, thank you for the help with the fixing of the reinforcement steel and the mixing of the concrete, as well as Adriaan Fouche for helping me to understand the Zwick testing machine and its software and Arno Mohr for the help with the calibration of the Aramis system.

Lastly I want to thank the Lord for the guidance and help He gave me in this two years.

# Table of Contents

# List of Figures

# List of Tables

## Abbreviations

| | | |
|---|---|---|
| 2D | - | Two Dimensional |
| 3D | - | Three Dimensional |
| CFRP | - | Carbon Fibre Reinforced Polymer |
| DIANA | - | Non-Linear Analysis Software from Holland |
| DOF | - | Degree's Of Freedom |
| FE | - | Finite Element |
| FEA | - | Finite Element Analyses |
| FRP | - | Fibre Reinforced Polymer |
| L6BEN | - | Two node beam element in DIANA |
| L8IF | - | Four node interface element in DIANA |
| m | - | Metre |
| mm | - | Millimetre |
| NRD | - | Normalised Relative Displacement |
| Q8MEM | - | Four node quadrilateral element in DIANA |
| RC | - | Reinforced Concrete |
| μm | - | Micro metre |

# Chapter 1: Introduction

There is a constant need to keep structures lasting longer before they have to be replaced. The design structural lifetime of bridges varies depending on the use and reasons they were built. Bridges are usually used for transportation, but can also be used to support a pipeline, a waterway for barge traffic as well as overhead power lines. Such Infrastructure is usually designed for 100 years, Eurocode basis of design (EN 1990) as summarised in Table 1.

**Table 1: Indicative design working life (EN 1990)**

| Design working life category | Indicative design working life (years) | Examples |
|---|---|---|
| 1 | 10 | Temporary structures (1) |
| 2 | 10 to 25 | Replaceable structural parts, e.g. gantry girders, bearings |
| 3 | 15 to 30 | Acricultural and similar structures |
| 4 | 50 | Building structures and other common structures |
| 5 | 100 | Monumental building structures, bridges and other civil engineering structures |
| (1) Structures or parts of structures that can be dismantled with a view to being re-used should not be considered as temporary. | | |

This research studies a way to extend the structural life of bridges beyond its design life, or up to its design working life in cases of bridges that have deteriorated prematurely, or to improve the load bearing capacity due to reclassification or extension of the bridge traffic category or traffic load. As the most common function of a bridge is for facilitating transportation, this research is based on the cyclic loading effects caused by vehicles driving over bridges.

Carbon Fibre Reinforcement Polymers (CFRP) plates are mostly used in the aviation industry, but are also a good way of strengthening civil engineering structures. Extensive research has been done on CFRP plates used on buildings and other structures where static loads were applied, but not on cyclic loading and more specifically the effects caused by the cyclic loading on the bonding adhesive or epoxy and the plate itself in the region of cracks in the concrete it strengthens.

In 2009 Jacques Louw and Adriaan Badenhorst (Louw 2009; Badenhorst 2009) conducted tests on scaled beams to determine the effective bond length of the plates needed to sufficiently strengthen artificially damaged beams. Two types of cement were tested to

determine the bond characteristics of each type. The conclusion of the study was that OPC type (CEM I 42,5) cement performed slightly better thanSurebuild (CEM II 32,5) in terms of the bond and it was taken into consideration for this study.

To simulate debonding of CFRP plates from beams on smaller test specimens, an inverted concrete T-Section was designed and used for this study. The flange of the section was used to clamp it down while a CFRP plate bonded onto the face of the web was pulled off in shear-slip dominated mode by either subjecting the plate to a monotonously increasing load, or cyclic loading. Before the CFRP plate was applied to the concrete sections the concrete was cracked over the face of the web where the plate was applied, in order to allow debonding to be studied in the vicinity of a crack.

Under service conditions, bridges are usually allowed to have crack widths of 0.2-0.3 mm for durability, but often a crack width of 0.6-0.8mm realises. Such a crack width was chosen to account for damage caused before the section was repaired/strengthened by CFRP plates. As a scaled beam was used byLouw (2009) and Badenhorst (2009), the crack width was adjusted to 0.2 mm (Scale 1:4) to simulate the same conditions as for their research.

In addition to the physical tests, computational (finite element (FE)) modelling is used in this study to further investigate the debonding behaviour. For calibration of nonlinear models used in the FE analyses, experimental tests were carried out to determine the material properties of the epoxy, steel and concrete, but not for the CFRP plates, because no rupture was expected. Using these results, the T-section specimen response is analysed for both monotonous and cyclic loading to verify the computational models. Subsequently, also the scaled beam of Louw (2009) is analysed. The particular material model properties used by Louw were not determined in his work, so the same properties were assumed as determined in the current study, justified by use of the epoxy, CFRP and reinforcement steel that came from the same respective suppliers as for this study.

Reasonable simulation by Finite Element Analyses (FEA) of the observed physical behaviour justifies the use of the FE models to study debonding under various conditions, including cyclic loading at various load levels, to fill in gaps in experimental data and produce information relevant for a proposed design guideline for debonding under cyclic loading.

## 1.1 Scope

The work is limited to RC (Reinforced Concrete) beams under flexural conditions, both static and cyclic.

The scope of work is as follows:

i. To study debonding of CFRP plates in the vicinity of a flexural crack. Cracks dominantly caused by shear in RC beams are not considered.
ii. Limitations of parameters due to time constraint.
    a. A single, but typical concrete class 35 MPa (cube compressive strength).
    b. A single CFRP product and adhesive (epoxy) and application method.
    c. Typical laboratory conditions in terms of environmental climate (room temperature and relative humidity).
iii. Monotonous loading and cyclic loading were applied at quasi-static loading rates, so no dynamic effects of fast travelling vehicle wheel loads are considered.
iv. A limited number of specimens were tested for the various series of tests, limiting the statistical data basis to a bare minimum.

## 1.2 Thesis outline

The thesis layout is as follows. In Chapter 1, an overview including the background and scope of work is given. Chapter 2 presents a literature review of the static modes of failure for CFRP strengthened structures as well as design models, and fatigue modes of failure are also discussed. Some more background on this thesis is discussed in Chapter 3, in terms of work done previously at SU (Stellenbosch University) on strengthening RC structures with CFRP plates. In Chapter 4 the experimental approach to this study is described, which consists of the practical aspects of this thesis; the equipment used for the different tests that were designed as well as the results of all the tests. The computational approach to the study is discussed in Chapter 5, giving the background on material models and element choices for the FEA models that were built to simulate the experimental work of Chapter 4. In Chapter 6 the comparison between the experimental and computational approaches is discussed and in Chapter 7 guidelines are given for strengthening structures under cyclic loading and the conclusions of this study is given in Chapter 8.

# Chapter 2: Literature Review

Engineering models for analyses and design of CFRP-strengthening of infrastructure must capture physical mechanisms of failure, in order to be applicable or reasonably accurate. A vast pool of data is available due to extensive testing internationally of CFRP-strengthening, from which this research may benefit. In this chapter the relevant information is extracted and summarised, as it influenced the subsequent experimental design and methodology followed to study a particular debonding mode, namely in the vicinity of flexural cracks under cyclic loading.

## 2.1 Objectives of strengthening RC beams with FRP Laminates

The objectives of strengthening existing RC beams with FRP laminates may be one or a combination of the following (Buyukozturk et al. 2003):

- to increase axial, flexural or shear load capacities;
- to increase ductility for improved seismic performance;
- to increase stiffness for reduced deflections under service and design loads;
- to increase the remaining fatigue life and
- to increase durability against environmental effects.

## 2.2 General debonding problems of external FRP strengthened beams

Due to the increase in the strengthening objectives above the retrofitted structures are susceptible to the following failures because of the increase of its capacities.

There are several failure mechanisms for FRP strengthened RC beams. Depending on the beam and strengthening parameters as set out by Buyukozturk et al. (2003) failure may take place through:

- concrete crushing before yielding of the reinforcing steel;
- steel yielding followed by FRP rupture;
- steel yielding followed by concrete crushing;
- cover de-lamination and
- FRP debonding.

FRP strengthened beams usually debond in regions of high stress or strain concentrations (in the presence of a crack or material discontinuities). The propagation path of debonding initiated by stress concentrations is dependent on the elastic and strength properties of the repair and substrate materials as well as its interface fracture properties. Theoretically, debonding in FRP strengthened beams can take place within or at the interfaces of materials that form the strengthening system, favouring a propagation path that requires the least amount of energy (Buyukozturk et al. 2003).

The different models of debonding are discussed in the next section (Section 2.3) it is also linked to the different failure modes listed above.

## 2.3 Static models

FRP strengthened structures under static loading has been researched to the extent that different models of debonding can be defined due to the different modes of failure.

### 2.3.1 Existing models for debonding

#### 2.3.1.1 Shear capacity based model

In a study by Smith and Teng (2002) they investigated 3 models for shear capacity and the conclusion they came to is that the debonding failure strength is related to the shear strength in concrete with no or partial contribution by the shear steel reinforcement. For the models investigated they did not consider the interfacial stresses between the FRP laminate and the concrete (Smith and Teng, 2002).

#### 2.3.1.2 Concrete tooth model

A concrete tooth model is when a “tooth” is formed between two adjacent cracks (Smith and Teng 2002). The tooth deforms like a cantilever beam under the action of the horizontal shear stresses at the base of the retrofitted beam. The FRP debonds when the tensile stresses at the “root of the tooth” (near the tension steel reinforcement in the beam) will exceed the tensile strength of the concrete. This results in a piece of concrete breaking out of the beam. The results from the investigated models (Smith and Teng 2002) were that an effective length can be determined for end anchorage over which a uniform shear stress is assumed.

#### 2.3.1.3 Interfacial stress model

A popular and logical assumption is that concrete cover separation or plate end interfacial debonding is due to high interfacial stresses at the end of the FRP plate (Smith and Teng 2002). Generally, interfacial stress debonding models make use of closed-form solutions and a concrete failure criterion, but some of these models investigated by Smith and Teng (2002) make use of the ACI concrete code (ACI 318-95, 1999) to predict the shear capacity of the retrofitted RC beam. They concluded that the stirrup efficiency factor is related to the peak interfacial stresses at the FRP end. These models combine the interfacial stresses and the shear capacity approach.

#### 2.3.1.4 Local bond-slip model

An FEA model was built (Jiang et al. 2004) to study the local bond-slip behaviour in the interface. From the analysis the stress and the slip in the FRP plate could be calculated at any point along the plate. The interfacial shear stress can then be deduced from the longitudinal stresses in the plate. To develop the bond-slip model, a finite element parametric study was performed to get the relationships between (1) various bond parameters, (2) geometric parameters and (3) material parameters. The study showed that the local maximum bond strength and the corresponding slip are almost linearly related to the tensile strength of concrete, while the total interfacial fracture energy is almost linearly related to the square root of the tensile strength in concrete.

### 2.3.2 Failure modes

#### 2.3.2.1 Classification of Failure Modes

The following classifications of failure modes are the most common for FRP strengthened structures (Teng et al. 2002). The failure modes are classified into these seven main categories (Figure 1):

- Flexural failure by FRP rupture
- Flexural failure by crushing of concrete
- Shear failure
- Concrete cover separation
- Plate-end interfacial debonding
- Intermediate flexural crack-induced interfacial debonding and
- Intermediate flexural shear crack-induced interfacial debonding

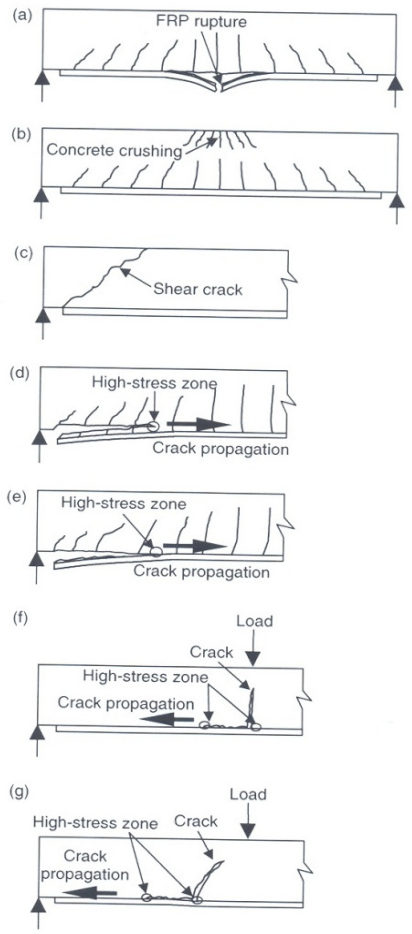


**Figure 1: Failure modes of FRP-plated RC Beams (Teng et al. 2002)**

Each failure mode listed is discussed below.

#### 2.3.2.2 Flexural failure

The ultimate flexural capacity of a retrofitted beam is reached when the FRP plate fails by tensile rupture of the FRP plate (Figure 1a) or the concrete is crushed in compressive region (Figure 1b). FRP rupture generally occurs following the yielding of the longitudinal reinforcement steel. When an RC beam is strengthened in flexure with FRP plates the beam gains strength and become less ductile. (Teng et al. 2002)

#### 2.3.2.3 Shear failure

A flexural strengthened beam can fail in shear, which is by nature a brittle failure mode (Figure 1c). The shear mode of a RC beam can be made critical by flexural strengthening. Because the FRP plate provides little resistance to shear, shear strengthening of the beam must be done simultaneously to ensure the flexural strength is not compromised. (Teng et al. 2002)

The beam ends can be wrapped using a multi-directional CFRP wrap, but this is not the aim of the study and was therefore not applied.

#### 2.3.2.4 Plate-end debonding

Strengthened RC beams can fail before the ultimate flexural capacity is reached. This premature failure is due to the debonding of the FRP plate. There are two modes of failure: (i) Concrete Cover Separation and (ii) Plate-end interfacial debonding (most common) as illustrated in Figure 2.

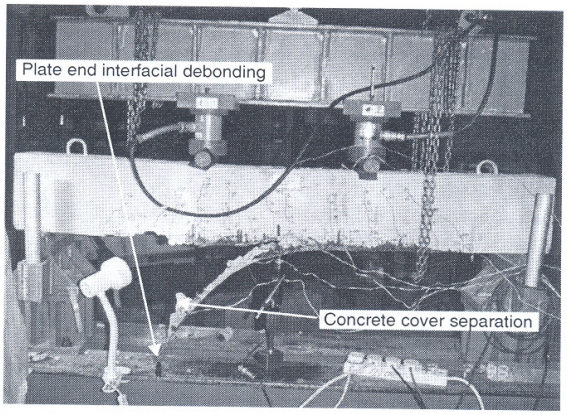


**Figure 2: Plate-end debonding failures (Teng et al. 2002)**

#### 2.3.2.4.1 Concrete Cover Separation

This failure occurs away from the bond line (adhesive layer) near the end of the FRP plate due to high stress concentrations (Figure 1d and Figure 2). Failure is initiated by the formation of a crack at or near the plate end. This is caused by high interfacial shear and normal stresses at that point.

#### 2.3.2.4.2 Plate-end Interfacial Debonding

This failure occurs in the bond line (adhesive layer) near the end of the FRP plate (Figure 1e). The load-deflection response for this mode of failure is similar to that of concrete cover separation. A thin layer of concrete generally remains on the debonded plate suggesting that the failure occurred in the concrete substrate adjacent to the concrete-to-adhesive interface.

### 2.3.2.5 Intermediate crack-induced interfacial debonding

#### 2.3.2.5.1 Intermediate Flexural Crack-Induced Interfacial Debonding

Flexural crack induced debonding occurs when a vertical (flexural) crack is formed. When a crack forms it releases tensile stresses from the concrete and is transferred to the FRP plate, resulting in high local interfacial stresses between the FRP plate and the concrete next to the adhesive layer. As the applied load increases; the interfacial stresses increase resulting in propagation of the crack towards one of the plate ends (Figure 1f).
(Teng et al. 2002)

#### 2.3.2.5.2 Intermediate Flexural Shear Crack-Induced Interfacial Debonding

This mode of debonding is almost the same as flexural crack–induced debonding (above). In this case a flexural shear crack (Figure 1g) is responsible for the debonding due to peeling stresses on the FRP plate-to-concrete interface. It is believed by Teng et al. (2002) that the widening of the crack is normally the more important factor.

#### 2.3.2.6 Other debonding failure modes

Combinations of the failure modes described above can also occur. Another possible mode of failure is inter-laminar shear failure within the FRP plate, but this mode does not appear to have been reported in tests to date (Teng et al. 2002).

#### 2.3.2.7 Summary of failures

The models and failures discussed in section 2.3.1 and 2.3.2 can be summarized as follow:

**Table 2: Failures models**

| Model | Failures |
|---|---|
| Shear Capacity Based Models | Plate-end De-bonding Failure |
| | Intermediate Flexural Shear Crack-induced Interfacial De-bonding |
| Concrete Tooth Models | Concrete Cover Seperation |
| | Intermediate Flexural Crack-induced Interfacial De-bonding |
| Interfacial Stress Based Models | Plate-end De-bonding Failure |
| Local Bond-Slip Models | Crack-induced Interfacial De-bonding |

## 2.4 Cyclic models

Extensive research has been done on CFRP strengthened structures that is subjected to monotonic load, but limited work has been done on cyclic loading and fatigue. The failure modes of static/monotonic loading models were discussed briefly in previous sections, but there are no particular fatigue failure modes or design models as yet. It cannot be assumed that models derived from monotonic, static tests are applicable under cyclic conditions, leading to fatigue. Fatigue testing of CFRP strengthened structures (beams) has been carried out to determine the governing factors of fatigue failure.

Brief descriptions of some tests are given below.

El-Tawil et al. (2001) simulated accelerated fatigue behaviour of RC beams strengthened with CFRP plates. Their method was implemented in a computer program that accounted for the nonlinear time-dependent response of the composite system. From the internal stresses obtained from their model it showed that cyclic fatigue leads to an internal redistribution of stresses similar to that obtained under static creep. (El-Tawil et al. 2001)

Barnes and Mays (1999) conducted experiments to see what the stresses in the CFRP plate is compared to the stresses in the reinforcement steel. Three loading options were used: (1) apply the same load to both CFRP strengthened and normal RC beams, (2) apply loads to give the same stress range in the rebar in both types of beams, and (3) apply the respective percentage of the ultimate load capacity to each beam. Their findings were that fatigue fracture of the internal reinforcement is the dominant factor of failure under fatigue loading (Barnes and Mays, 1999).

In another study set out by Aidoo et al. (2002) the objective was to determine whether external FRP repair methods are able to resist fatigue loads and to establish what the effect is that these repair systems have on the fatigue behaviour of bridge girders. The outcome was that the fatigue behaviour of such retrofitted beams is controlled by the fatigue behaviour of the reinforcing steel, but the fatigue life can be increased by the application of an FRP plate, which relieves some of the stress carried by the steel. (Aidoo et al. 2002)

The studies done by Barnes and Mays (2009) and Aidoo et al (2002) indicated that the governing factor of fatigue failure of FRP strengthened structures is the fatigue behaviour of the reinforcing steel after the FRP plate debonded, but they did not investigate the effects that caused the FRP plate to debond.

The aim of the research was to determine what the effect of each cycle of fatigue/cyclic loading has on a CFRP strengthened RC structure.

The intended result is that one can get a design equation to determine debonding per loading cycle at different force amplitudes or to limit the number of cycles for a given stress range.

# Chapter 3: Background to this thesis

## 3.1 Louw and Badenhorst cyclic tests

Louw (2009) conducted research on the cyclic loading effects on CFRP strengthened bridge beams where the CFRP plate was bonded on the full length of the beam (Louw, 2009). The beams' effective length was 3 m long, the depth 225 mm and width 150 mm. These dimensions were determined from scaling a typical bridge beam (12 m x 900 mm x 600 mm). The calculated tensile reinforcement of the scaled beam was 484mm$^2$ and 7Y10 reinforcement bars were used which had an area of 550mm$^2$.

Some of the beams were artificially damaged by grinding through 3 of the 7 bars in the middle of the beams to simulate damage due to accidents or rust resulting in a loss of 43% in tensile reinforcement. The beams were then reinforced with CFRP strips at the bottom so that the resisting moment of the CFRP beams is nearly the same as the resisting moment of the reference beams.

Louw also conducted a static test on a reference beam (beam with no damage) and a CFRP strengthened beam where he applied a monotonic load. The stiffness of the elastic part of deformation is the same and the peak forces of the two beams are in the same range (Figure 3).

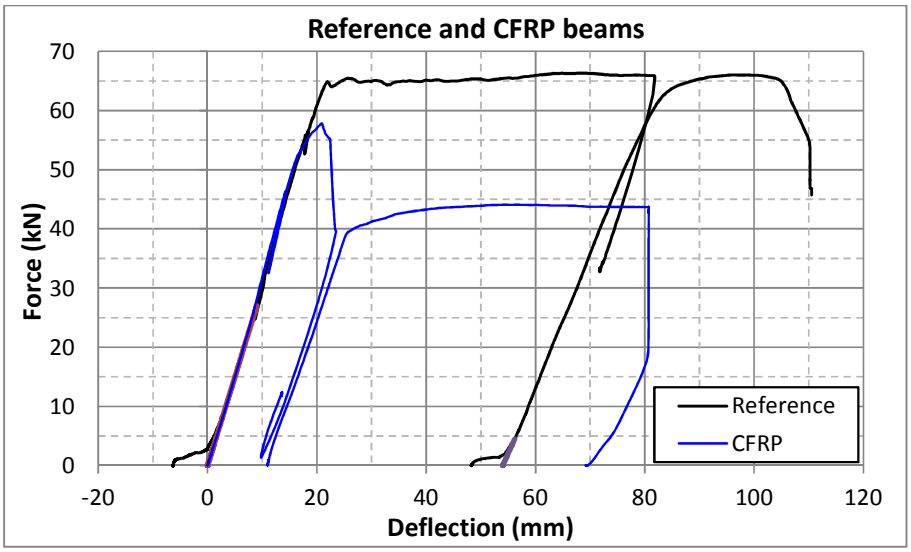


**Figure 3: Monotonic load response graphs (Louw, 2009)**

Badenhorst (2009) tested the use of different types of cement (OPC and Surebuild, CEM I and CEM II respectively) and it indicated that the OPC type cement (Figure 4, b) was better to use because more concrete and stone bonded to the beam than the Surebuild (CEM II) beams (Figure 4, a) thus bonding the CFRP plate more effectively to the concrete substrate.

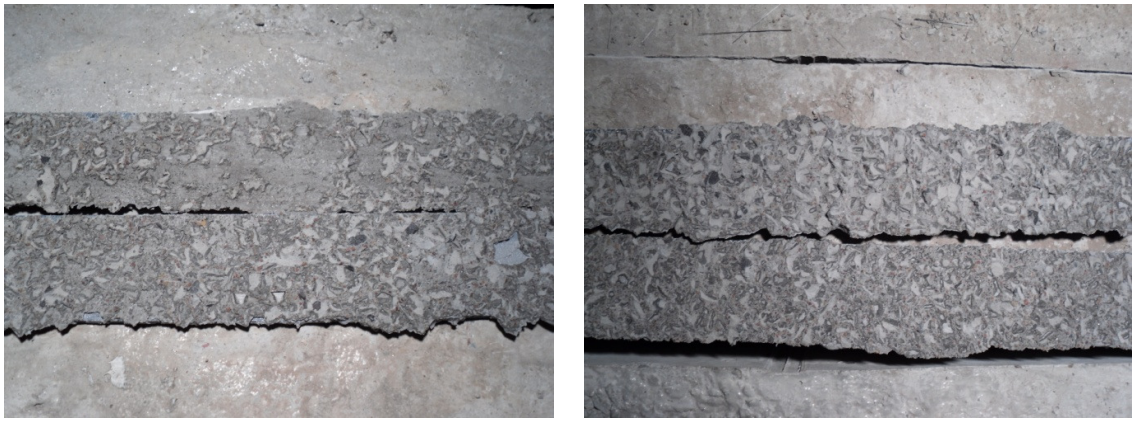

**(a) CEM II 32.5 – based concrete substrate (b) CEM I 42.5 – based concrete substrate**

**Figure 4: Delaminated CFRP strips (Badenhorst, 2009)**

Because of the better bonding of the OPC (CEM I) cement it was decided that it would be used for this research. The beams tested under monotonic load by Louw (2009) was also analysed (Section 5.6) as a case study to validate the analyses of the other tests. Apart from the analytical case study of the beam other experimental tests were also designed, tested and compared to computational analyses.

# Chapter 4: Experimental approach

For all the experimental tests the material were tested to obtain an accurate representation of the values used in the computational analyses of the different tests. Concrete cubes were tested to get the representative strength of larger specimens. The reinforcement steel was tested in a previous study, but the yield stress of the steel is relevant for the analyses in Chapter 5. The properties of the epoxy and CFRP plates are taken from the suppliers' specification. The epoxy (adhesive) strength is also tested by way of a triplet shear test, which is usually performed to determine the bond between two bricks with a mortar joint. Experiments were designed and performed at various levels, from small tests which isolate individual mechanisms to intermediate size tests which simulate dominant failure mechanisms to allow a feasible experimental program to large beams for validation. The following sections describe the total experimental programme at each of the levels.

## 4.1 Material properties

### 4.1.1 Concrete

For all the test samples, 3 cubes were cast to determine if the consistency of the mixes are the same. 3 cylinders were also cast because DIANA (Nonlinear analysis software) use cylinder compressive strength of the concrete instead of cube compressive strength because it is a more accurate representation of what happens in a beam or a larger structure. Cube compressive strength is an over estimation of the true value due to confining of the boundary conditions that falsely represent the true strength. The concrete mix design is discussed in Appendix A.

#### 4.1.1.1 Cube results

Three concrete cubes were cast with all the experimental specimens to get a representative average compressive strength of the concrete. The cubes were crushed at the same time as the larger specimens were tested. The age of the tests varied from 28 days to 35 days. The triplet shear tests were done at 28 days and the static and cyclic tests of the T-sections were done after 35 days. The cube compressive strength values are given in Table 3.

**Table 3: Concrete cube compressive strength**

| Test | Mix_Specimen no. | Cube Comp. Strength (MPa) | Average Comp. Strength (MPa) | Std. dev. (MPa) |
|---|---|---|---|---|
| Triplet | All Specimen | 45.0 | 44.3 | 1.1 |
| | | 44.8 | | |
| | | 43.1 | | |
| Pull-off tests for bond tensile strength | 1_1 | 41.4 | 40.2 | 1.3 |
| | | 39.2 | | |
| | | 39.9 | | |
| | 2_2 | 43.7 | 43.4 | 0.9 |
| | | 42.3 | | |
| | | 44.1 | | |
| 85% Cycles | 1_3 | 43.1 | 44.5 | 1.3 |
| | | 45.1 | | |
| | | 45.2 | | |
| 65% Cycles | 2_2 | 47.5 | 46.4 | 1.0 |
| | | 46.1 | | |
| | | 45.7 | | |

#### 4.1.1.2 Cylinder results

Due to time constraint the cylinders were tested after 7 days to get the 7 day strength (Figure 5) to start the final analyses. The cube results (which were tested on the day of the experimental tests) were adjusted according to the Eurocode 2 (BS EN 1992-1, 2004) to get the cylinder strength at 28 days which was used in DIANA.

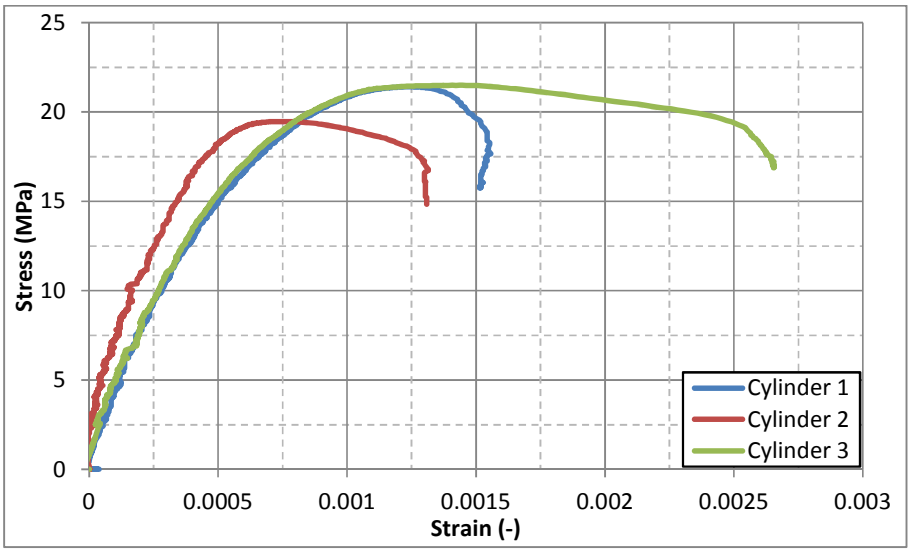


**Figure 5: Concrete cylinder test results (7 day strength)**

The 3 cylinders that were tested yielded values relatively close to each other. The purpose of recording the full stress-strain response is to capture the nonlinear model for FE analyses. The shape of cylinder 3 was used for the analyses. The different points along the graph used were (Table 4):

**Table 4: Stress - Strain relationship of concrete cylinders**

| Stress (MPa) | Strain (-) |
|---|---|
| -3.28725 | -0.00009 |
| -5.35092 | -0.00011 |
| -19.29404 | -0.00078 |
| -20.33198 | -0.00090 |
| -20.39195 | -0.00091 |
| -21.37374 | -0.00115 |
| -21.49738 | -0.00145 |
| -19.27150 | -0.00252 |
| -17.68681 | -0.00223 |

Note that the sign convention of compression being negative is used.

### 4.1.2 Steel

Badenhorst (2009) tested Y10 reinforcement steel (Figure 6) and as the steel came from the same supplier one can assume that the tensile strength response of the steel used subsequently was similar.

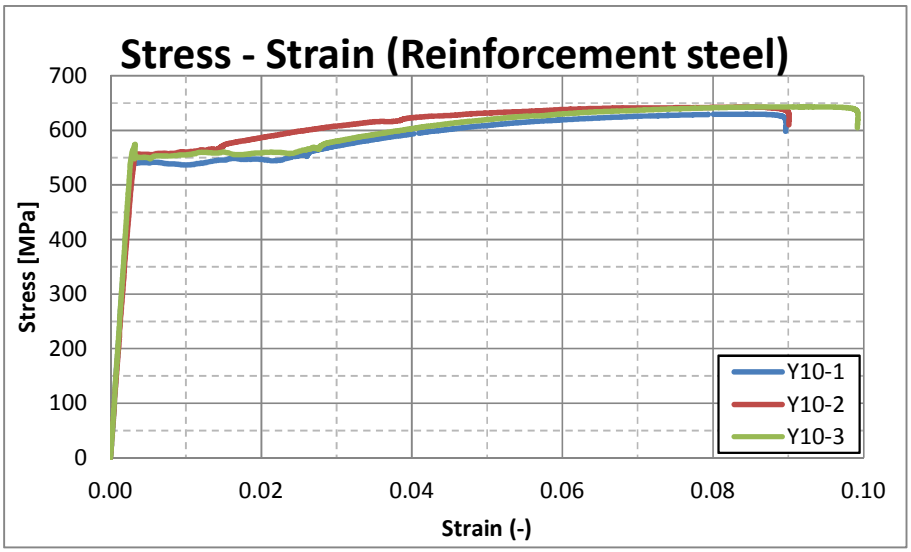


**Figure 6: Stress - Strain relationship of reinforcement steel (Badenhorst, 2009)**

The input required by DIANA for the reinforcement steel is the tensile strength at the start of the plastic zone and the ultimate strength before rupture (Table 5). The yield criterion used is based on von Mises plasticity and linear hardening was assumed for the reinforcement in the analyses.

**Table 5: Stress - Strain relationship of Y10 reinforcement for DIANA**

| Stress (MPa) | Strain (-) |
|---|---|
| 550.00 | 0.00 |
| 640.00 | 0.09 |

Note that the sign convention of tension being positive is used.

### 4.1.3 Epoxy and CFRP plates

The epoxy (Table 6) and CFRP plates (Table 7) used was sponsored by Mapei South Africa (Pty) Ltd and the strengths were given by the supplier.

**Table 6: Epoxy properties**

| Supplier: MAPEI | |
|---|---|
| E-Modulus | 4 GPa |
| Tensile strength (7 days) | 30 MPa |
| Shear strength | 3 MPa |
| Service temp (°C) | 5 tot 30 |

**Table 7: CFRP plate**

| Supplier: MAPEI | |
|---|---|
| Carboplate E200 | |
| E-Modulus | 200 GPa |
| Tensile strength | 3300 MPa |
| Width (mm) | 50 |
| Thickness (mm) | 1.4 |

The CFRP plates for the research did not rupture in any of the tests in this project, so the strength properties given by the supplier were considered to be sufficient for analyses. Tests were conducted to verify the given shear strength of the epoxy because it is suggested to be the same as the bond strength to the concrete (section 4.3).

## 4.2 Apparatus used for testing

### 4.2.1 Zwick Z250 testing machine and software

The Zwick Z250 testing machine has the capability to handle forces up to 250kN in either tension or compression. Various test configurations can be set up in the machine. By removing the bottom clamp as shown in Figure 7 one can clamp down a test specimen to the travelling base plate. The machine also has its own software that can be programmed to control the speed of the test, the control method as well as the minimum and maximum forces required to perform cyclic tests.

**Figure 7: Zwick Z250 testing machine**

### 4.2.2 LVDT`s

HBM W10 LVDT`s (linear variable displacement transducers) (Figure 8) were used for all the experiments. For the cylinder compression tests three LVDT`s were used to get the average displacement which was then divided by its original gauge length to get the strain.

**Figure 8: LVDT - Linear Variable Displacement Transducer**

For the triplet and T-Section tests the configuration of the setup is described in Section 4.3 and Section 4.5 respectively.

### 4.2.3 Spider8

Spider8 (Figure 9) converts analogue data obtained from LVDT`s and load cells to digital data which can be used to draw graphs. This was used with LVDT`s to plot the compression strength vs. strain of the concrete cylinders.


**Figure 9: Spider8**

### 4.2.4 Contest testing machine

The Contest testing machine (Figure 10) is used to test concrete cubes and cylinders. The machine uses force controlled load application at a constant rate of 180kN per minute.

**Figure 10: Contest Testing Machine**

Used in conjunction with LVDT`s and the Spider8 the average strain over the gauge length at any average stress obtained from the load cell force reading can be calculated. Typical results of the test method are given for the cylinder compressive strength in Figure (Section 4.1.1.2).

### 4.2.5 Aramis

The Aramisoptical measurement system consists of 2 cameras (Figure 11, left) mounted at an angle to get 3 dimensional (3D) pictures to be prepared from the photos of test specimens. To get the deformation from said specimen, the specimen must first be painted white, usually with lime powder mixed in water. Once the mixture is dry a black speckle pattern must be sprayed on the specimen (Figure 11, right) for the Aramissystem to determine the deformation, based on the well-contrasted speckle pattern.

**Figure 11: Aramis and test specimen**

From this speckle pattern Aramis keeps track of how the individual dots move relative to each other and in turn the deformation can be calculated which is performed by the software.

## 4.3 Test 1 – Triplet Shear Tests

A triplet shear test was carried out to verify the shear strength and cohesion of the epoxy which bonds the CFRP plate to the concrete. The setup was simulated in the computational approach, but roller supports were used instead of no tension interfaces or Teflon bearings.

The specimens consists two 25 mm steel plates bonded onto concrete on each side. The concrete was 42 mm thick while the height and width of all the specimens were 150 mm x 150 mm. The bonded area on one side of the specimen was 110 mm x 110 mm to ensure that one side breaks away before the other. The concrete was cast in the same manner as the other tests and the curing time was the same as for Test 3. The age of the concrete at the time of testing were 28 days; 14 days in water, 7 days drying time at which point the steel plates were bonded onto it and 7 days after that the specimens were tested.

Two different measurements were taken during testing with the LVDT`s (Section 4.2.2). Both measurements were taken on the side where the epoxy area was smaller. The vertical displacement (Figure 12a) was used to control the tests at a constant rate of 1.5 mm per minute. The diagonal displacement (Figure 12b) was also measured to see if there was any rotation of the specimen.

**a.) Vertical displacement** **(b) Diagonal displacement**

**Figure 12: Triplet Shear Experimental Setup**

Figure 13 shows a tested triplet specimen that debonded the same way as the T-sections (Section 4.5) as well as the smaller bonded area.

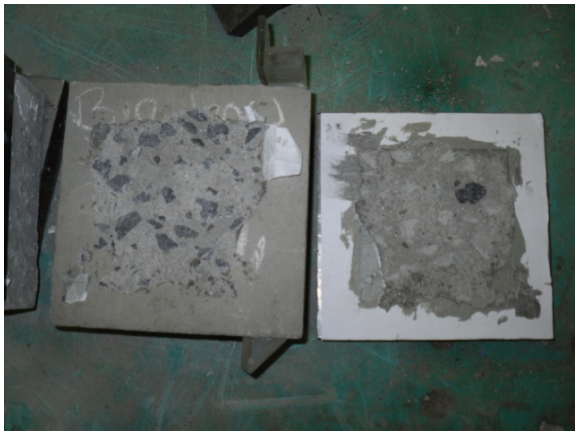

**Figure 13: Tested triplet specimen**

The vertical displacement was plotted against the shear stress (Figure 14). The stress was determined by taking the total force that acted on the specimen and then divided by two to get the reaction force of the support. The layout of the setup is the same as for a simply supported beam thus the reactions on both sides are equal to each other. The scaled force was then divided by the area to get the shear stress on the side with the smaller bond.

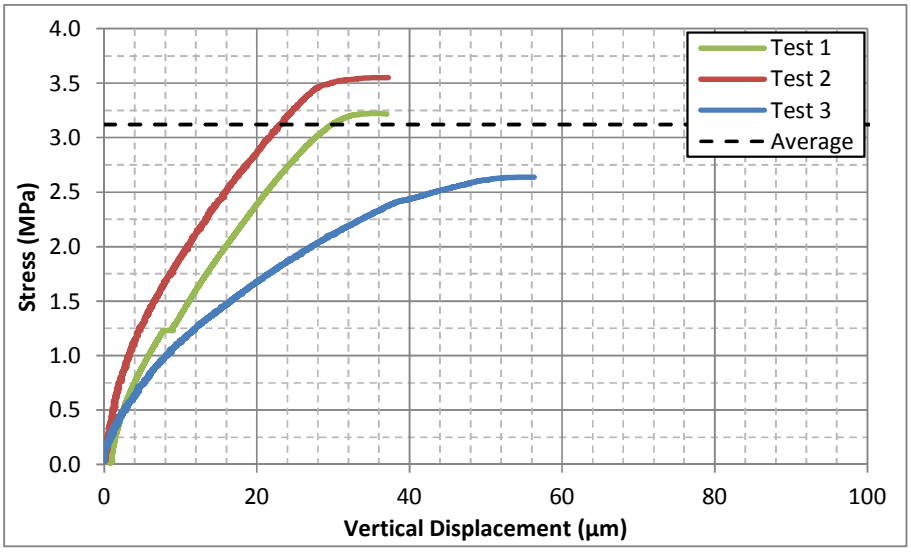


**Figure 14: Zwick Triplet response graph**

From the experimental results an average value for the shear strength of the epoxy is taken as 3.1MPa which is a bit higher as what the manufacturer specified.

## 4.4 Test 2 – Louw and Badenhorst Beam Experiment

The beams Louw (2009) tested were scaled bridge beams under static and cyclic loading. The dimensions of the beams were 225 mm x 150 mm x 3400 mm (h x w x L), it was reinforced with 7 Y10 steel bars in the tensile zone and it was externally strengthened by a 50 mm x 1.4 mm CFRP plate bonded onto the bottom of the beams spanning the entire unsupported length of 3 metres. The beam was freely supported on rubber pads so the ends were free to lift (rotate) due to the applied force in the centre. Figure 15 shows where the supports were and where the loading was applied.

**Figure 15: Louw (2009) experimental setup**

The concrete had average compressive strength of 39.57MPa at 28 days (Louw, 2009) when the beams were tested.

Figure 16 shows the experimental force-deflection response graph of a CFRP strengthened beam tested by Louw (2009) under monotonic load. After the debonding of the CFRP plate from the concrete, the applied load was taken to zero to get the permanent displacement of the debonded beam.

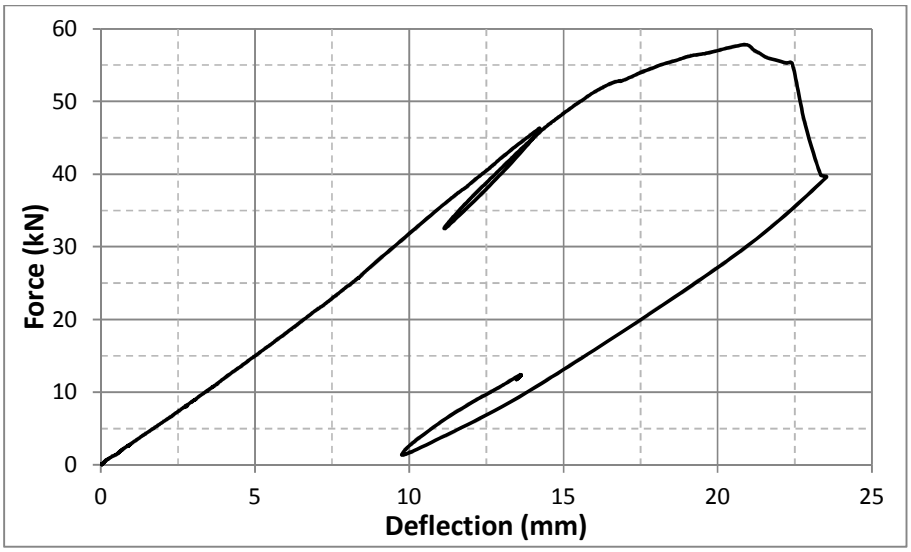


**Figure 16: Louw experimental response graph (Louw, 2009)**

This test was the basis for the cyclic tests done by Louw (2009). The ultimate resistance force of the beam was 57 kN and subsequently cyclic tests on other, similar beams prepared in the exact same way were done at 67% of this ultimate force to simulate serviceability loading conditions.

The beam is a good case study to analyse and see whether the epoxy strength tested in section 4.3 is accurate enough to use as input values for the final T-section test discussed in the next section.

## 4.5 Test 3 – Inverted T-Section

The main aim of this study is to develop a model for cyclic debonding in the vicinity of a crack. An experiment was designed to see how the CFRP plate transfers the stresses over one crack of a concrete specimen. A 3D layout of the specimen is given in Figure 17. The inverted T-Section was used because of the practicality of the specimen, it is small, relatively easy to handle and it fits into the Zwick Z250 testing machine. The position of the crack is 100 mm from the top of the concrete as indicated in Figure 17.

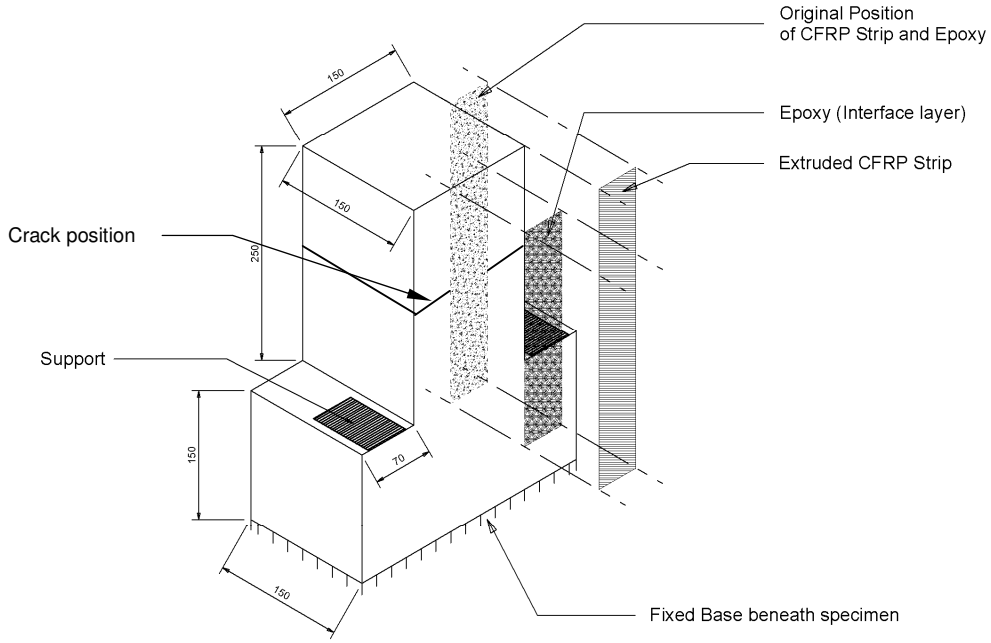


**Figure 17: 3D Model layout**

Normal pull-off tests were done first to determine the overall load-deformation response to enable calibration and final input values of the analyses, but also the force levels for subsequent cyclic tests on similar specimens. There after the cyclic tests were set up in the same manner as the static (pull-off) tests.

All the specimens were handled in the same manner and they were pre-cracked by tensile loading in the Zwick, by gripping steel bars extending from the specimens. This was done before the CFRP plate was applied. Two LVDT`s were used during this pre-cracking to measure the crack opening over a notch in the section as shown in Figure 18. The setup was controlled by one LVDT and had a limit of 0.2 mm. Once the limit has been reached the test stops.

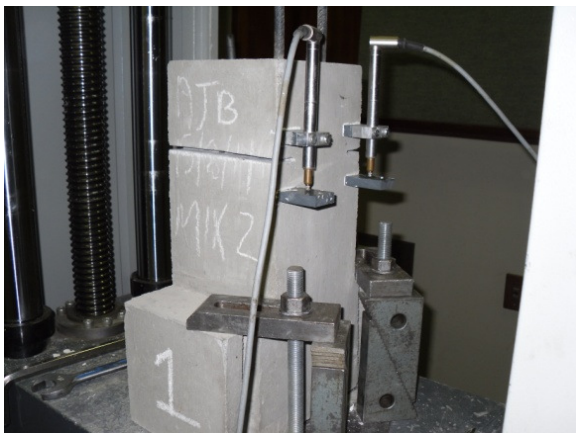

**Figure 18: Cracking of T-Section**

The T-Section for the experimental pull-off and cyclic tests were set up with the bonded face of the concrete to the front of the machine as shown in Figure 19(left). The face of the specimen was painted white with lime and a black speckle pattern was sprayed on for the Aramis system to measure the displacement.

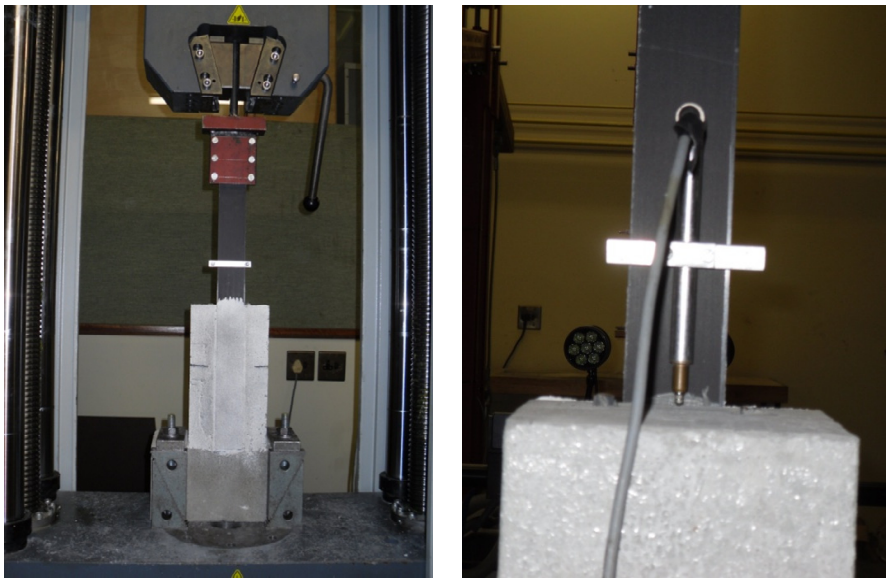

**Figure 19: T-Section experimental setup**

The CFRP plate was clamped at the top with the help of a purposely made clamp and the clamps at the base were bolted down with two Grade 8.8 M16 bolts which weretorque to 200 kNm. The reason for the specific torque is just for a reference so that every tested specimen has the same boundary condition. For every specimen the same margin of lift can be assumed before the force is applied.

The pull-off tests were displacement controlled by the LVDT clamped to the back of the CFRP plate and pushed onto the top of the concrete (Figure 19, right) to get the global displacement.

Cyclic loading can best be described as caused by vehicles passing over a bridge that cause the bridge to deflect and return to almost the same initial position. As the number of cycles imposed on the beam increases the permanent deflection of the beam increases. Civil engineering structures of this type are designed to withstand loads imposed repetitively on the structure, thus the cyclic load level is taken as a percentage of the maximum force the structure can support and not a percentage of the maximum deflection of the beam.

For cyclic tests the general displacement vs. time graph is given in Figure 20. It shows that the initial displacement grows fast (stage I) until the structure is adjusted to the imposed loads, then it reduces in growth (stage II) until just before it breaks or debonds (stage III) when the displacement increases rapidly until the structure fails.

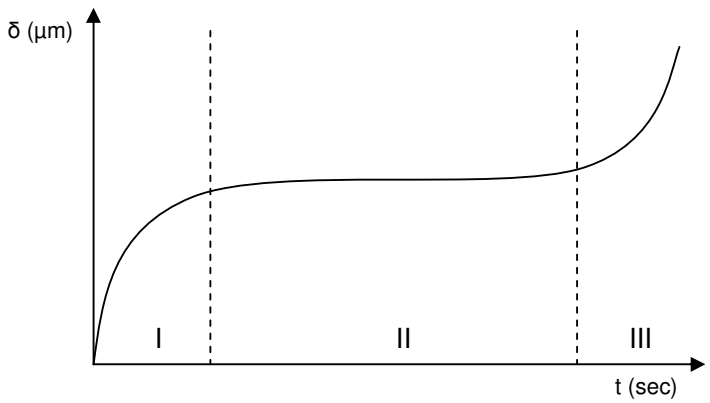


**Figure 20: Displacement vs. Time**

Cyclic tests were carried out at two different amplitudes, 85% and 65% of the pull-off force. The reason for the two different amplitudes is to see what the influence of the force level is on the structure, the number of cycles that can be resisted and the increase in permanent deformation induced at different load levels. The 85% cyclic test is for near ultimate conditions whereas the 65% test is to simulate more reasonable serviceability conditions. This is nevertheless a high cyclic load, justified by the requirement to limit the number of cycles to failure for feasible experimental testing. The aim is to simulate the behaviour computationally, after which more reasonable service loads can be simulated in DIANA, for development of design recommendations.

According to Al-Hammoud et al. (2011) who tested simply supported beams, the minimum load can be as little as 8% of the maximum static load capacity so that the beam would not slip or bounce. The minimum load used for the cycles in this study was taken as 10% of the pull-off force. Because of the direct tensile stress on the CFRP plate the decision was made to increase the minimum load from 8 to 10% on the section to ensure that the structure remains in tension.

### 4.5.1 Test 3 – Results

#### 4.5.1.1 Static loading

Two specimens were tested under static loading one from each batch mixed with the exact same ingredients and ingredient amounts, as well as in the same mixer, but mix two mixed after completion of mix one. The reason for the difference in the ultimate response of the two specimens can be attributed to the difference in the concrete strength (Section 4.1.1).The two tests had almost the same displacement at debonding (Figure 21) and the rapid loss in resistance is shown for Test 1_1. The stress is plotted against the displacement because of the difference in bonding area of the CFRP onto the concrete. The stress is simply the force divided by the bonded area, this was done for a better representation of the results and it was found that the bonded area has a big influence on the maximum force.

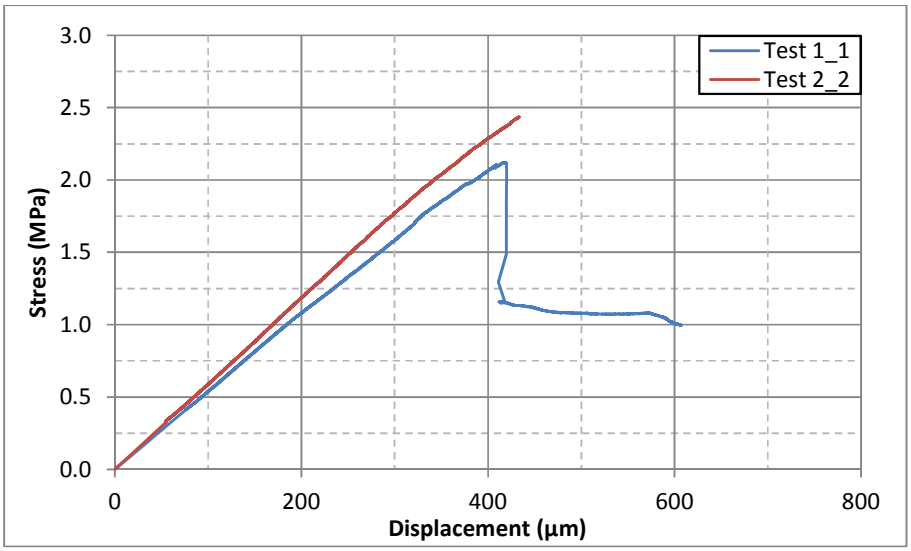


**Figure 21: Zwick Pull-off tests on T-section specimens (Test 3)**

The peak stress of the two samples was in reasonable agreement as seen in Figure 21. This test was analysed by FE analysis, as discussed in section 5.7.2.1.

After completion of the pull-off tests the bonded areas were carefully studied and measured on the CFRP plate. The overall length of bonded area was not perfectly controlled but varied with up to 5 mm. Also un-bonded or poorly bonded areas left areas without concrete parts attached to the plate. The overall area was determined and the un-bonded areas subtracted leading to the results in Table 8.

**Table 8: Pull-off tests bond area**

| Pull off Tests | | Total Area ($mm^2$) | Bonded Area ($mm^2$) | Max. Force (N) | Stress (MPa) | Ave stdev |
|---|---|---|---|---|---|---|
| Cracked | 1-1 | 15400 | 14575 | 30897.88 | 2.12 | 2.2849 |
| | 2-2 | 15675 | 15516 | 38011.31 | 2.45 | 0.2333 |

The bonded areas for the two tests are given in Table 8. From the average stress it was scaled to 85% and 65% for the cyclic tests to get the force amplitude required.

With the help from the Aramis system, the relative displacement between the CFRP plate and the concrete were determined. The step showed in Figure 22 is for Tests 2_2 not at the peak force because the Aramis system could not capture a photo at that point in time due to 2 reasons namely; (1) the sample rate of the photos taken is one per second and (2) because of the rapid debonding the system could not define any reference points at the peak force.

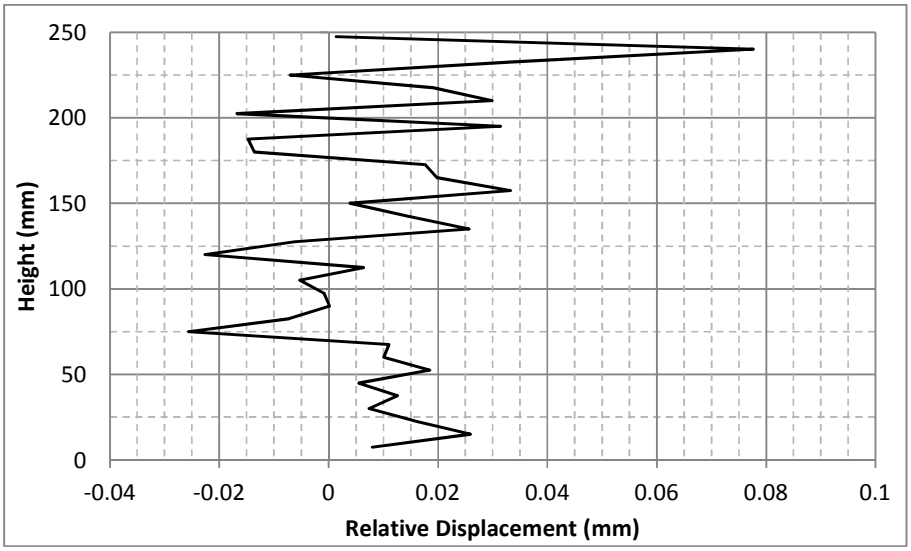


**Figure 22: Aramis relative displacement between CFRP and concrete**

There is a 0.02 mm "jump" in the vicinity of the crack position at the height of 150 mm of the specimen. The Aramis displacement is compared to the Diana displacement in section 6.3.1. The stress level at which this graph is plotted is 2 MPa, which is near the peak stress, where debonding occurs, of the T-section.

#### 4.5.1.2 Cyclic loading

##### 4.5.1.2.1 Cycles at 85% of pull-off force

For this test 26 cycles were completed and the CFRP plate debonded in the loading stage of the last cycle. The delamination growth per cycle is not clearly visible in Figure 23 because of the number of data points in the graph. The other problem with this setup is that the CFRP plate on which the LVDT was clamped bended (rotated) during the unloading of each cycle making the unloading line of the graph crossing the loading line. The curve of the unloading (visible in the first cycle) is a confirmation of the bending of the CFRP plate. The curve is a result of slight rotation of the LVDT, for the initial loading (cycle 1) the line is straight suggesting no rotation.

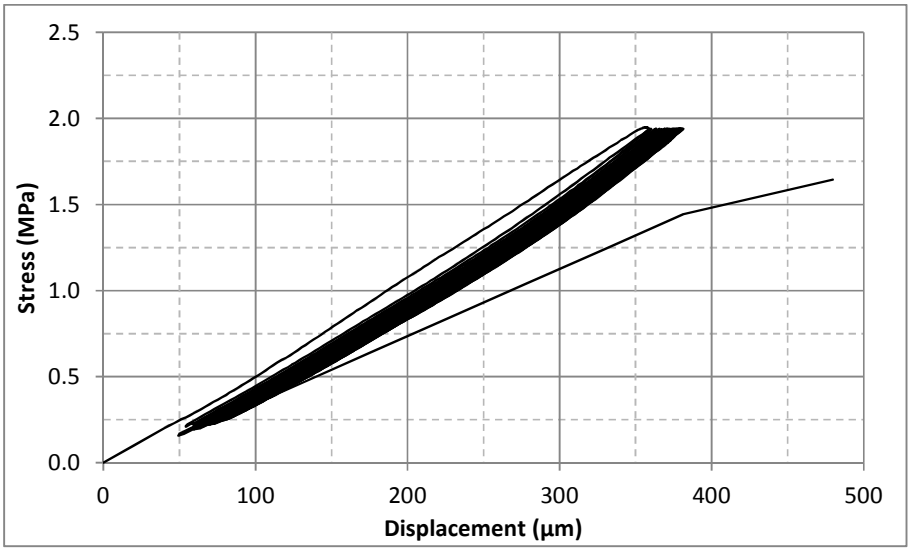


**Figure 23: Zwick 85% Cycles response curve**

Unfortunately the Aramis system was tampered with before this test and it was assumed that the system was still calibrated correctly. After the test when the data was analysed it was found that the data do not correspond with the computational data and thus it was concluded that the data obtained by the Aramis system for this test cannot be used.

The bond area was also measured after the test, like for the pull-off test, and it was found that the guessed area was close to the actual bonded area and resulted that the test was done at 84.8% of the pull-off test (Table 9).

**Table 9: 85% Cycles test bond area**

| 85% Cyclic tests | | Total Area ($mm^2$) | Guessed Bonded Area ($mm^2$) | Cyclic Force (N) | *Guessed Stress (MPa) | Actual Bonded Area ($mm^2$) | Actual Stress (MPa) | Percentage of Pull-off test (%) |
|---|---|---|---|---|---|---|---|---|
| Cracked | 1-3 | 15125 | 14646 | 28446 | 1.94 | 14675 | 1.94 | 84.8 |

*An assumption of actual bonded area had to be made in order to select a cyclic force level, as the bonded area can only be studied accurately after completion of a test.

Although the displacements in the local coordinate system could not be measured with the Aramis system, the number of cycles and the percentage of the force amplitude are close to the FE analysis done in section 5.7.2.2.1.

#### 4.5.1.2.2 Cycles at 65% of pull-off force

For the 65% cyclic tests the first cycle has a similar large initial displacement as for the 85% cyclic tests (Figure 24). The total number of cycles for this test is 300, after which no delamination is observed. The test was stopped at that point because it was observed that the permanent displacement of the specimen was almost non-existent and due to the amount of data that had to be analysed. From this observation it seems that the force amplitude is low enough that the specimen is under the static creep limit (El Tawil et al., 2001) and that failure will occur only after a huge number of cycles.

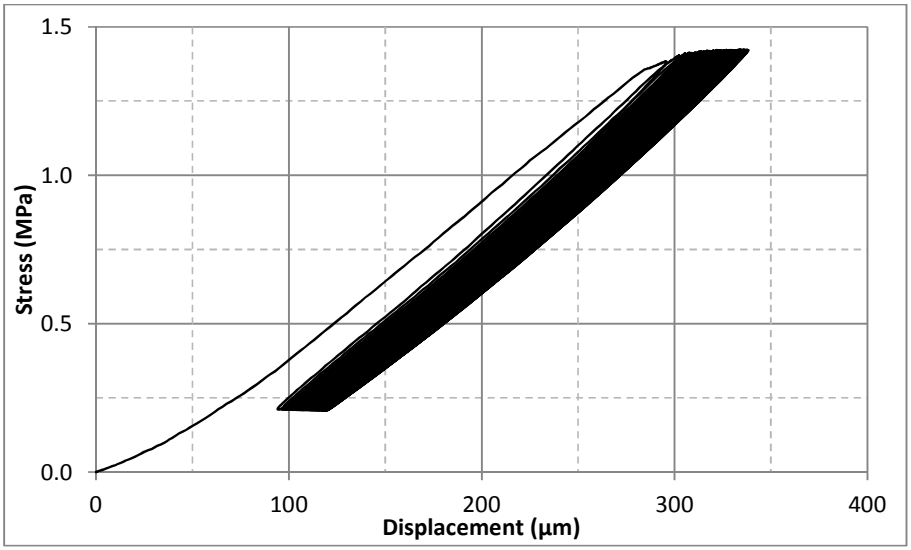


**Figure 24: Zwick 65% Cycles response curve**

The intended 65% of the pull-off force was not reached due to a larger bonded area than expected. The actual percentage at which the cycles were done was 63% (Table 10).

**Table 10: 65% Cycles test bond area**

| 65% Cyclic tests | | Total Area ($mm^2$) | Guessed Bonded Area ($mm^2$) | Cyclic Force (N) | *Guessed Stress (MPa) | Actual Bonded Area ($mm^2$) | Actual Stress (MPa) | Percentage of Pull-off test (%) |
|---|---|---|---|---|---|---|---|---|
| Cracked | 2-2 | 15125 | 14646 | 21753.06 | 1.49 | 15125 | 1.44 | 62.9 |

*An assumption of actual bonded area had to be made in order to select a cyclic force level, as the bonded area can only be studied accurately after completion of a test.

With the help of the Aramis system the local displacements can be shown over the height in the vicinity of the crack (150 mm). The delamination growth per cycle seems to be non-existent for this test as shown in Figure 25, except for small differences. The stress range for the test seems to be low enough that no or very little damage is done per loading cycle.

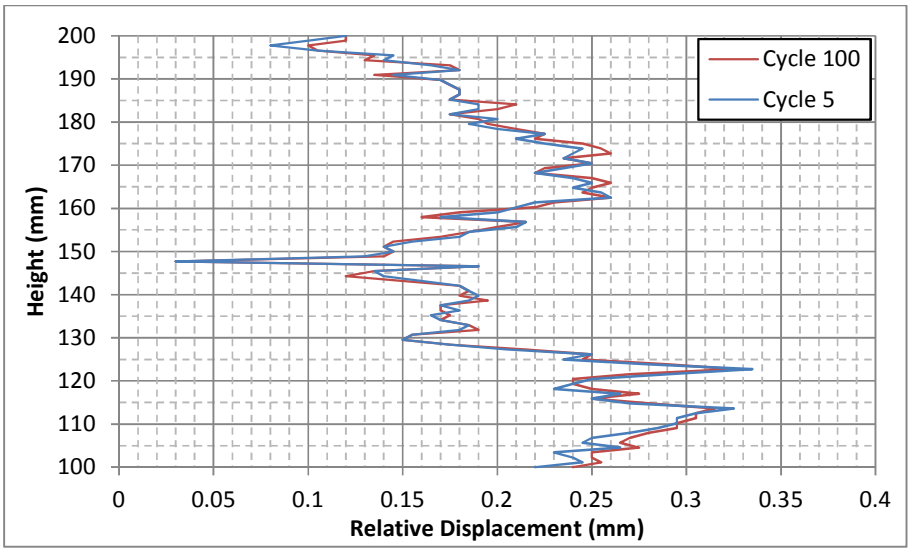


**Figure 25: Aramis relative displacement (65% test)**

## 4.6 Observed failure modes

There are 2 prominent failure modes observed during all the tests. The failure mode that was mostly seen was plate end debonding (Figure 26a) of the CFRP plate where the concrete near the interface was ripped out of the specimen and the other mode was concrete cover separation (Figure 26b) where an entire piece of concrete was broken off the sample so that the reinforcing steel is visible.

**a.) Plate end debonding**

**b.) Concrete cover separation**

**Figure 26: Observed failure modes**

# Chapter 5: Computational approach

## 5.1 Review on computational models

For the experimental part of this project an inverted RC T-Section was designed and used to bond a CFRP plate to the face of the web. The CFRP plate was extended above the concrete section to clamp the top of the plate in order to apply a load to the structure. The T-Section is cracked before the CFRP plate is bonded onto it.

A triplet test was also modelled to determine the shear strength (cohesion) of the epoxy that bonds the CFRP plate to the concrete. (See section 5.5)

The different material models, element choices and background on material responses are described below before the different tests are discussed.

### 5.1.1 Limit to elastic behaviour

The CFRP plates used in the analyses will not reach its elastic limit, because of its high tensile strength, despite the high modulus of elasticity. The epoxy which is modelled as an interface will deform until it “breaks away”/debonds from the CFRP plate. The concrete for the beam analysis will reach its elastic limit in the compression zone, thus a total strain crack model is used for the concrete which allows inelasticity in compression as well as tension. (See section 5.3.2)

### 5.1.2 Plasticity

#### 5.1.2.1 Concept of Yield function

Due to the relationship between vertical and horizontal loads shown in Figure 27 one can deduce a Normal – Shear stress relationship as in Figure 28.

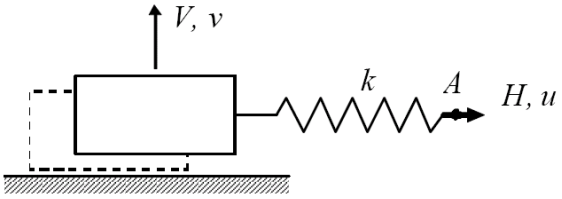


**Figure 27: Plastic response**

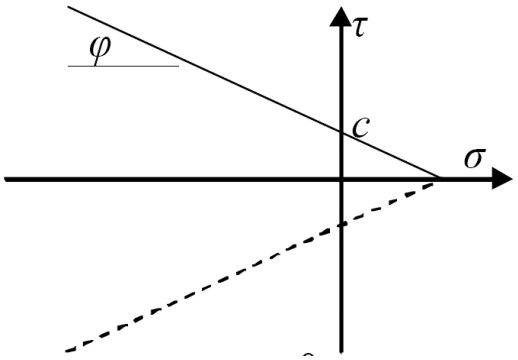


**Figure 28: Normal - Shear stress relationship**

This stress relationship graph gives a friction coefficient tan (φ) and adhesion (C) which can be measured in experimental tests. The adhesion (C) or shear resistance is the stress necessary to debond the CFRP plate from the concrete. This can also be described as the strength of the epoxy which glues the plate to the concrete.

The epoxy will start to debond as soon as it exceeds its limit strength. This will then be the starting point of debonding and it will spread along the applied CFRP plate until the whole length of the plate has debonded.

### 5.1.3 Interface mechanics

#### 5.1.3.1 Contact interfaces

The contact interface concept is when a contact problem arises i.e. the contact can be brought about by a roller support or roller/wheel rolling over a specimen. It can also be a bearing like a rubber pad on which a test specimen rests during testing. For the purpose of this study a contact interface was used in various ways which will be explained in more detail in the model schematisation of each model.

#### 5.1.3.2 Sliding friction

Sliding friction is where slip takes place between two surfaces (ex. shear cracks in concrete). It can also be a contact interface that slides along a discontinuity as shown in Figure 27. This is the ideal interface for the modelling the epoxy that glues the CFRP plate to the concrete.

### 5.1.4 Crack modelling

There are three basic modes of cracking;

I. Direct delamination,
II. Shear and
III. Twist. (Figure 29)

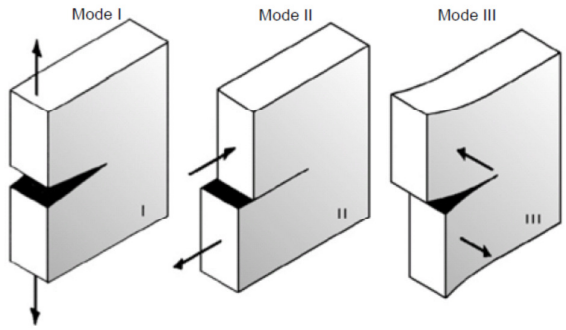


**Figure 29: Crack mode definition**

For the T-section model only crack mode I is applicable as the CFRP plate are pulled off from the concrete section as the forces will be in the same direction as shown (Figure 29). An opening in the crack position will also be modelled.

## 5.2 Element choice

The different analytical models that were developed for this study make use of different element and material models. The use of different elements and material models for each parameter of the tests are discussed below.

### 5.2.1 Concrete, steel clamps and plates

The chosen elements to model the concrete and steel clamps in DIANA are Q8MEM; four node quadrilateral elements (Figure 30). This is an isoparametric plane stress element which is based on linear interpolation and Gauss integration.

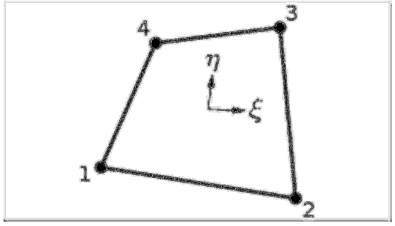


**Figure 30: Q8MEM element**
**(Diana 9.3, Element Library)**

This element requires an input of Young`s modulus, Poisson ratio and thickness. The strain $\varepsilon_{xx}$ is constant in the x direction and varies linearly in the y direction and the strain $\varepsilon_{yy}$ is constant in the y direction and varies linearly in the x direction (Diana 9.3, Element Library). Cracks cannot form in the element itself, thus a crack will form between 2 adjacent elements.

For accurate correlation between experimental and computational tests, the experimental value for Young's modulus and the average tensile and compressive strength of the concrete will be used in the finite element analysis as shown in (Section 4.1.1). The tensile and compressive strength of the concrete will also be used for the crack interfaces.

### 5.2.2 CFRP Plates and Steel bolts

The element of choice for the CFRP plates and bolts are L6BEN (straight, 2 node) elements (Diana 9.3, Element Library). These elements are two dimensional class I-Beam elements, with basic variables $u_x$, $u_y$ and $\varphi_z$, which are the displacements in the x and y directions, respectively, as well as the rotation around the z axis (Figure 31). The strain $\varepsilon_{xx}$ is constant and the curvature $K_z$ varies linearly along the centre line of the beam.

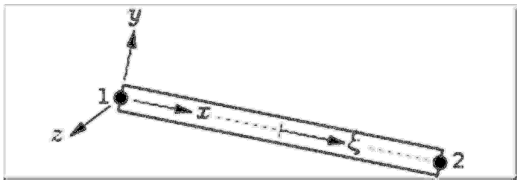


**Figure 31: L6BEN Element (Diana 9.3, Element Library)**

This element type requires geometrical input parameters; cross-section area and moment of inertia and material parameters; Young`s modulus and Poisson ratio. The CFRP and bolt parameters can be calculated from the experimental setup.

### 5.2.3 Epoxy interfaces

L8IF interface elements were used to model the no-tension base and the epoxy between the concrete and CFRP plate. The L8IF element in DIANA is an interface element between two lines in a two dimensional configuration (Diana 9.3, Element Library) as seen in Figure 32. This element is based on linear interpolation and a 3-point Newton-Cotes integration scheme. By default it has two displacements DOF (Degrees Of Freedom), but an additional rotation DOF can be added.

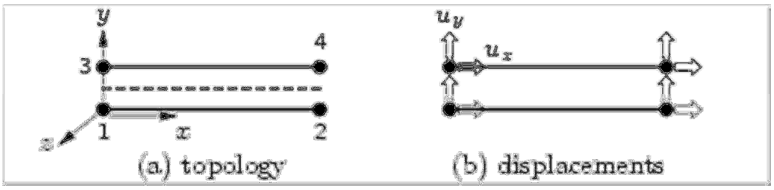


**Figure 32: L8IF Interface element (Diana 9.3, Element Library)**

With this interface element one can use different material models to modify its response in terms of stiffness, compressive and tensile strength and fracture energy. The default requirement is the stiffness.

### 5.2.4 Embedded Reinforcements (Rebar)

BAR elements were chosen to model the reinforcement bars that can be embedded in various families of elements; beams, solids, curved elements and plane stress elements. In finite element models, bar reinforcements have a shape of a line as shown in Figure 33a.

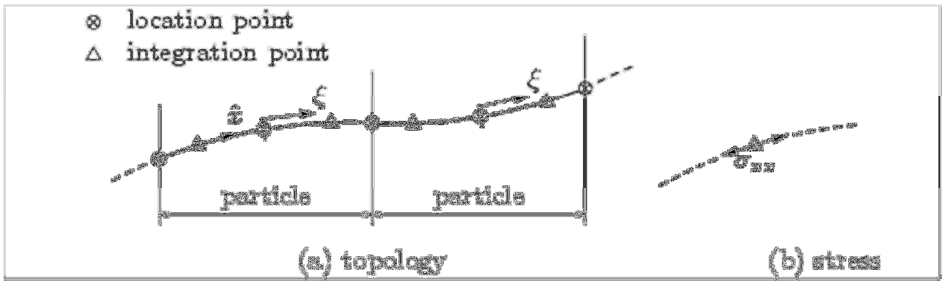


**Figure 33: Reinforcement bar (Diana 9.3, Element Library)**

The input data for the embedded elements is general material and geometric properties and the specification of the location of the bar. The yield criterion used for BAR elements is based on von Mises plasticity and linear hardening.

## 5.3 Material models used

The use of material models is to give certain properties to selected materials and in turn to different elements in the model. For most of the materials used in the analyses, the properties will remain linear, but there are some exceptions.

### 5.3.1 Composite Interface Model (Epoxy)

This interface material model is appropriate to simulate fracture, frictional slip as well as crushing along interfaces (Diana 9.3, Material Library). This material model was used as the epoxy which bonds the CFRP plate onto the concrete. Additional inputs are the Mode I and Mode II fracture energies, shear strength and tensile strength.

### 5.3.2 Total Strain Crack Model (Concrete)

The total strain crack model is used to simulate the tension softening behaviour of concrete and in turn show where cracks will form in a beam for instance (Diana 9.3, Material Library). There are a lot of different predefined models to be used (Figure 34), but Hordijk`s model (Figure 34f) is used for analyses in this project.

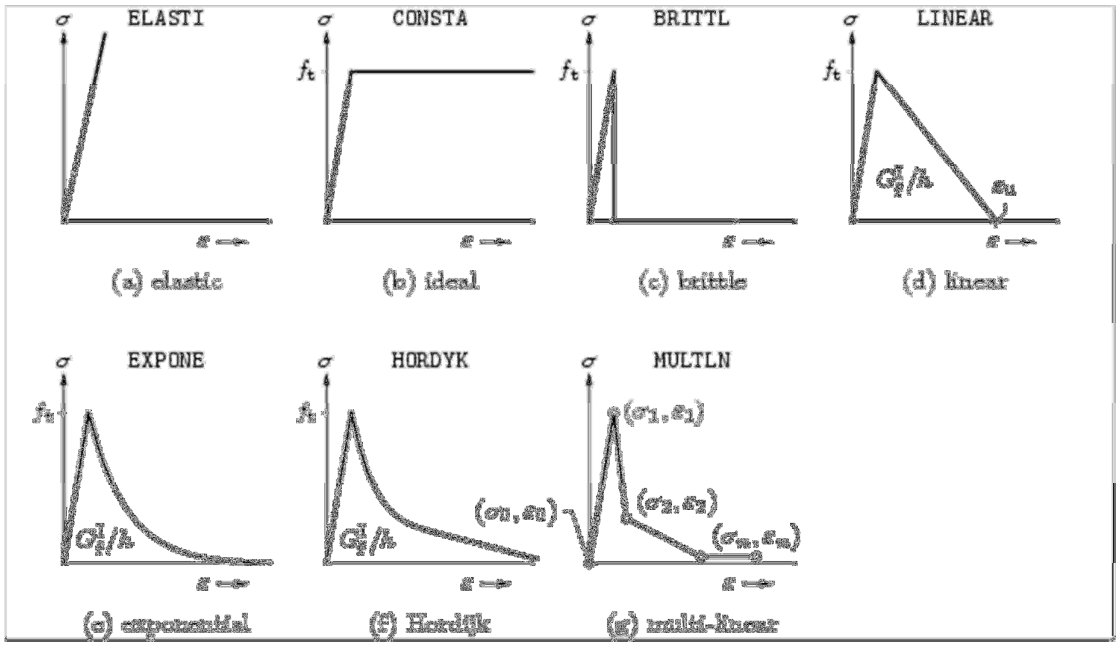


**Figure 34: Predefined tension softening for total strain crack model (Diana 9.3, Material Library)**

Additional input requirements for the model are the tensile strength and fracture energy of the material. These material models and element choices are mentioned in each computational model where applicable.

## 5.4 Control methods

There are two types of control methods used for tests; displacement control and force/load control (Figure 35).

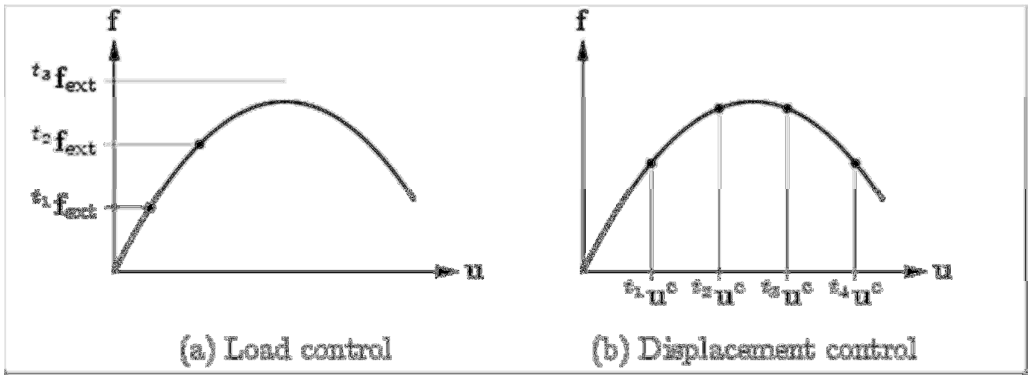


**Figure 35: Force and Displacement control (Diana 9.3)**

Displacement control is commonly used when the force response of a structure is unknown. For example the force will grow with the displacement in the elastic zone, but as soon as some of the elements starts to exceed its yield stress the displacement will still increase constantly (Figure 35b), but the force will increment less with each load step.

Force control is better to use when a targeted force is required like with cyclic tests. The force increment is constant (Figure 35a) while the displacement can vary along the path. With force control the stresses at failure can be better calculated and described because the stress path followed remains at a constant interval.

## 5.5 Test 1 – Triplet Shear Analyses

A triplet shear test is usually carried out by bonding 3 bricks with 2 mortar joints on each side of a centre brick. In principle the test can be used to bond two steel plates to concrete with epoxy (adhesive). The main objective of the test is to determine the shear strength or cohesion ($c_o$) of the epoxy.

### 5.5.1 Test 1 - Analyses setup and input

2 dimensional (2D) triplet shear analyses was carried out to verify the shear strength of the epoxy tested in section 4.3 and see how it correlates to the shear strength provided by Mapei South Africa (Pty) Ltd.

The analyses were done which consisted of two steel plates bonded by epoxy (interface) on each side of a piece of concrete as well as a loading plate on top of the concrete to spread the load evenly across the surface (Figure 36).

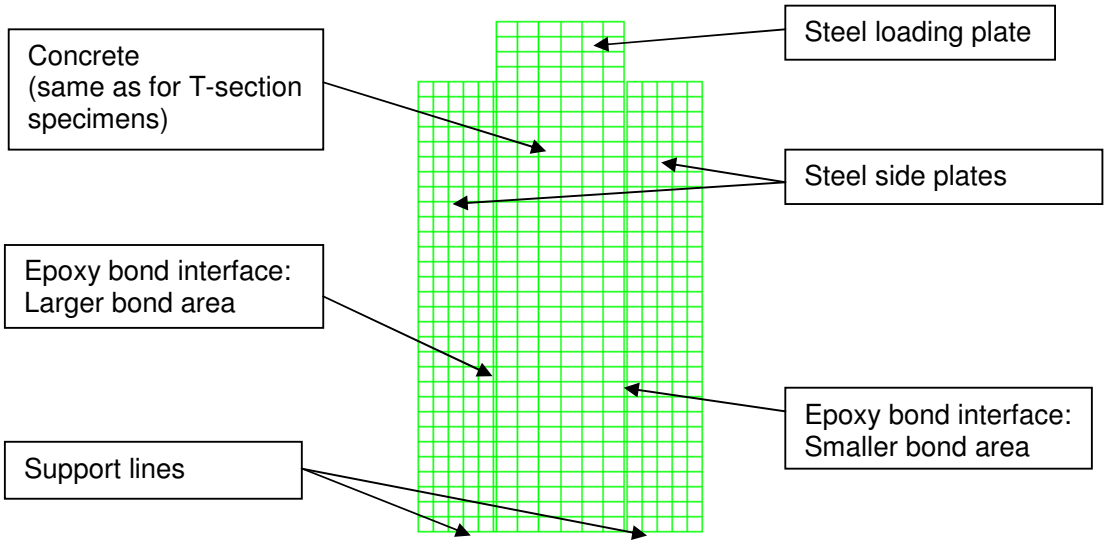


**Figure 36: Triplet computational layout**

At the support of the two side plates, a no-tension interface was inserted to simulate the roller support conditions which were the case for the experimental tests.

The concrete and steel plates (side and loading plates) were modelled with Q8MEM elements which are plane stress elements as defined in Diana. The epoxy and no-tension interface elements were L8IF elements. Refer to Sections 5.2.1 and 5.2.3 for element attributes.

Because it is a 2D (plane stress) analyses all the elements are given a depth (direction out of the page), width (horizontal axis) and height (vertical axis) to represent the actual 3D experimental design.

Geometrical inputs for the model were:

| | | |
|---|---|---|
| Depth of all elements: | | 150mm, unless otherwise stated. |
| Concrete: | Width: | 42mm |
| | Height: | 150mm |
| Steel plates (Side): | Width: | 25mm |
| | Height: | 150mm |
| Loading plate: | Width: | 42 mm |
| | Height: | 25mm |

The thickness of the epoxy on each side is 1mm and the height and width of the 2 sides differ. On the left side the whole area was bonded (150 mm x 150 mm) and on the right an area almost 55% of the total area, which in turn is 110mm x 110mm.

General material input values required for the analysis were:

Concrete:

| | | |
|---|---|---|
| Young`s modulus | – | 24.1 GPa |
| Poisson`s ratio | – | 0.2 |

Epoxy:

| | | |
|---|---|---|
| Normal stiffness | – | 110MPa |
| Tangential stiffness | – | 65 MPa |
| Mode I fracture energy | – | 0.0452 N/mm |
| Mode II fracture energy | – | 0.35 N/mm |
| Compressive strength | – | 37 MPa |
| Shear strength | – | 3.105 MPa |
| Tensile strength | – | 3.105 MPa |

Steel:

| | | |
|---|---|---|
| Young`s modulus | – | 210 GPa |
| Poisson`s ratio | – | 0.25 |

Values for the fracture energies were obtained from the experimental tests which were then improved, or fitted indirectly by changing the values until the graph represents the graph obtained from the experimental tests (Section 4.3).

The test was displacement controlled. The step increment was 0.05 mm over a 100 steps, however due to the different input values each analysis diverged after different number of steps. The top of the loading plate was used to transfer the displacement (applying the load) at the centre node on top of the loading plate, the master node, the other nodes acted as slave nodes to displace the same as the master. Master and slave nodes are a system used if there is a single action on a set of elements, but the distribution comes from one node in a defined line and the other nodes follow the same action.

### 5.5.2 Test 1 – Results

Out of 3 analyses of the triplet shear setup it was determined that the average shear strength of the epoxy is just over 3.0 MPa. Figure 37 shows the results obtained from the analyses. For the triplet shear analyses the Mode II fracture energy was given an average value for all the analyses, while the Mode I fracture energy and shear strength of the epoxy varied (Table 11).

**Table 11: Triplet fracture energies**

| | Test 1 | Test 2 | Test 3 | Average |
|---|---|---|---|---|
| Mode I Fracture energy | 0.0348 | 0.0208 | 0.0800 | 0.0452 |
| Mode II Fracture energy | 0.35 | 0.35 | 0.35 | 0.35 |
| Shear strength | 3.2 | 3.5 | 2.62 | 3.11 |

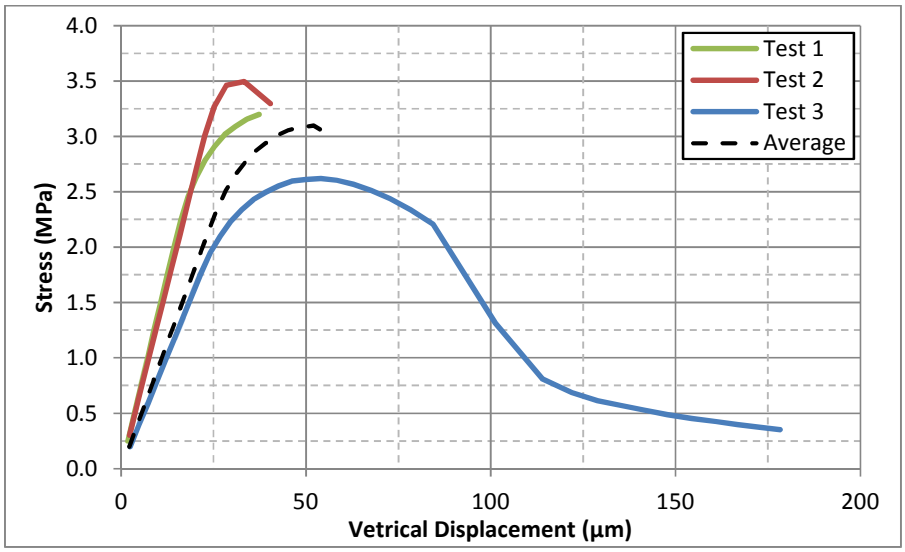


**Figure 37: DIANA Triplet analyses**

From the results obtained from the triplet shear analyses one can assume that the shear strength of the epoxy given by the supplier is sufficient for the other analyses. The mode I and mode II fracture energies can also be taken as sufficient to use in the case study of Louw`s (2009) beam and T-section tests.

## 5.6 Test 2 – Louw and Badenhorst Beam Analysis

### 5.6.1 Test 2 - Analysis setup and input

A computational model was designed to simulate the actual experimental test conducted by Louw (2009). The experiment was a simulation of a scaled bridge beam. The scaled beam was simply supported on two rubber pads, and the load was applied trough a loading plate on top of the beam at the centre of the span (3-point bending test).

The model layout of the analysis is the same as the experimental setup (Section4.4). A steel plate at the top of the beam where the force acts, the rubber pads at the bottom that acts as supports and a no tension interface between the rubber pads and the concrete were modelled so the ends are free to lift upward due to the load in the centre. The tensile reinforcement was also included in the analyses because it adds to the stiffness of the beam and reduces the probability that cracks will form in the initial loading stage. The model outline is shown in Figure 38.

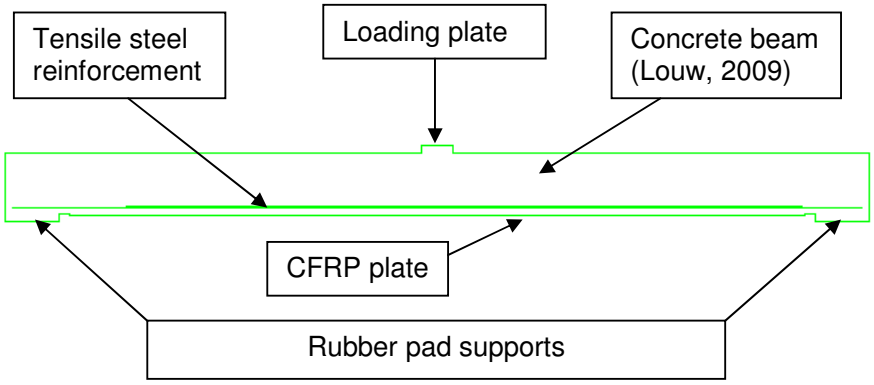


**Figure 38: Model layout of experimental beam**

There are various input parameters that had to be taken into account to get the same results as the experimental tests. The input parameters of the reinforcement steel, concrete and epoxy were determined through experimental tests as discussed in section 4.1 and the CFRP plate strength used was given by the supplier. The steel plate used for the loading plate was given nominal values for the elastic modulus and Poisson's ratio.

The analysis was displacement controlled to get the failure envelope of the beam. The displacement was incrementally enlarged to 25 mm over 100 load steps, i.e. 0.25 mm per step.

The element choices were Q8MEM elements for the concrete, rubber pads and loading plate (Section 5.2.1). L8IF interface elements were used for the epoxy (Section 5.2.3); L6BEN elements for the CFRP plate (Section 5.2.2) and BAR elements for the embedded reinforcement (Section 5.2.4).

Geometrical inputs for the model were:

Note: same notation for model layout as section 5.5.1.

| | | |
|---|---|---|
| Depth of all elements: | | 150mm, unless otherwise stated. |
| Concrete beam: | Width: | 3400mm |
| | Height: | 225mm |
| Rubber supports: | Width: | 200mm |
| | Height: | 5mm |
| Loading plate: | Width: | 120mm |
| | Height: | 25mm |
| Reinforcement steel: | Area: | 550mm$^2$, except at centre of span (324mm$^2$). |
| | Length: | Varies from 1575mm to 3350mm |
| CFRP plate: | Area: | 70mm$^2$ |
| | Length: | 2960mm |

The thickness of the epoxy between the concrete and CFRP plate is 1.0mm and the depth is 50 mm. The Q8MEM element size were 20mm (wide) with a varying height from 5mm to 25 mm, the L6BEN length were 20mm to connect to the concrete elements. The embedded reinforcement was only given the total length.

Material input values required for the analysis were:

Concrete:

| | | |
|---|---|---|
| Young`s modulus | – | 24.1 GPa |
| Poisson`s ratio | – | 0.2 |

Epoxy:

| | | |
|---|---|---|
| Mode I fracture energy | – | 0.0452 N/mm |
| Mode II fracture energy | – | 0.35 N/mm |
| Compressive strength | – | 39.5MPa |
| Shear strength | – | 3.105 MPa |
| Tensile strength | – | 3.95 MPa |

Steel:

| | | |
|---|---|---|
| Young`s modulus | – | 210 GPa |
| Poisson`s ratio | – | 0.25 |

The total strain crack material model used for the analysis requires a failure envelope for the concrete (Table 12) as well as a tensile strength.

The concrete envelope for the beam analysis is:

**Table 12: Compressive failure envelope for the concrete of the beam**

| Stress (MPa) | Strain (-) |
|---|---|
| -9.75513 | -0.00011 |
| -19.6201 | -0.00029 |
| -35.5118 | -0.00078 |
| -37.4448 | -0.00092 |
| -39.4675 | -0.00141 |
| -37.438 | -0.00091 |
| -33.9707 | -0.00258 |
| -32.416 | -0.00263 |
| -30.9781 | -0.00265 |

Note that the sign convention of compression being negative is used.

### 5.6.2 Test 2 – Result

In Figure 39 the force vs. displacement response graph shows that just after the peak force the force drops suddenly because of the debonding of the CFRP plate from the concrete at the bottom of the beam. The force drop is because of the loss of resistance the beam had.

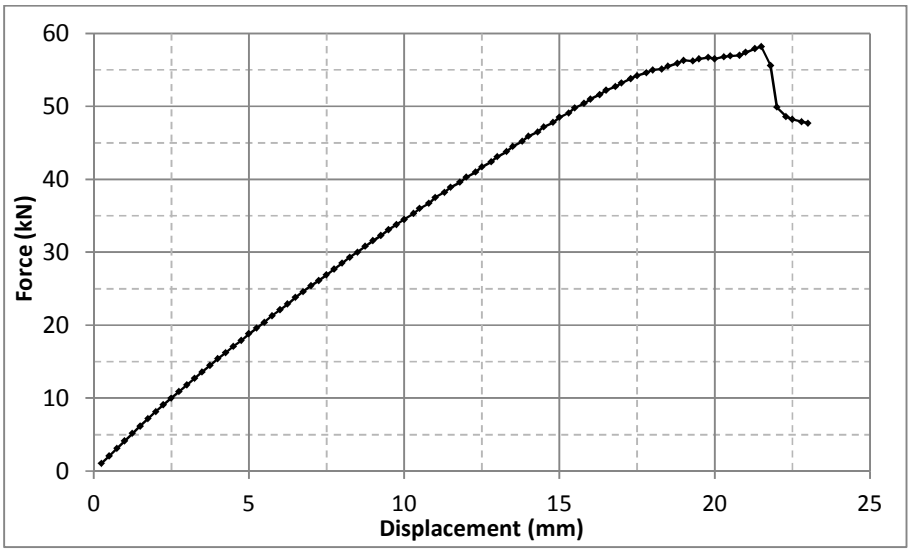


**Figure 39: DIANA Beam analysis**

Louw (2009) observed cracks at a constant interval of 6-7 cm throughout the length of the beam; the same observation was made with the modelled beam (Figure 40). This is a function of the choice of element size in smeared cracking analysis including the crack band formulation as employed here. This justifies the particular element size used for the analysis.

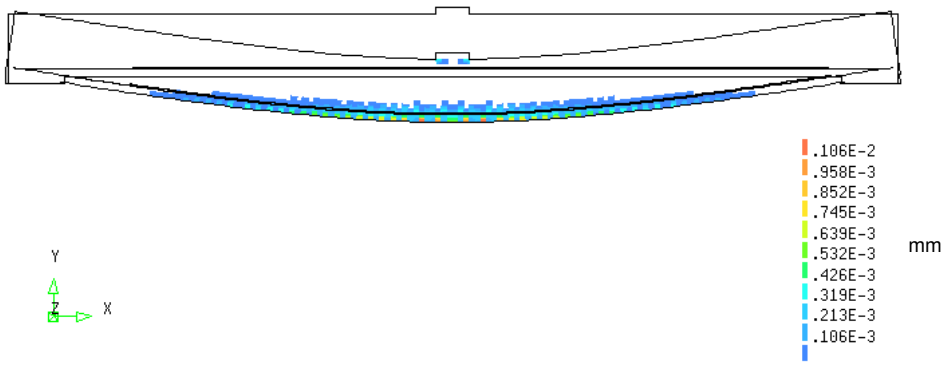


**Figure 40: Crack formation over beam**

The stiffness of the beam as it nears the peak force reduces because of the opening of the cracks in the concrete. After load step 6 the beam starts to crack and at the peak force (step 86) before debonding cracks are formed almost over the entire length of the beam (Figure 40).

From the reasonable comparison between the physical experimental response and the analysed response (see Chapter 6), it is concluded that the stiffness and strength parameters of the epoxy tested in section 5.5 are confirmed.

## 5.7 Test 3 – Inverted T-section Analyses

From the verification of the shear strength and fracture energies of the epoxy as well as the result obtained from the case study the material properties can be seen as an accurate representation of the true strength thereof. These values can be inserted into the final T-Section model.

The inverted concrete T-section was used to investigate the debonding of CFRP plates over a single crack.

### 5.7.1 Test 3 – Analysis setup and input

The computational setup was based on the experimental tests in every aspect and was taken into account. The material model properties were all the same as for the beam analysis (Section5.6).

The interface elements are L8IF interface elements as discussed in Section 5.1.3. The CFRP plate and M16 bolts are L6BEN beam elements (Section 5.2.2). The rest, concrete and steel clamps, are Q8MEM membrane elements (Section 5.2.1).

The method of load application is displacement control for the static test and force control for the cyclic tests.

It has the following model parameters:

- No tension interface at the base of the model to simulate a loose standing structure that is clamped down.
- Two steel M16 bolts and clamp plate to hold down the structure.
- Crack opening at pre-determined position.
- Steel reinforcement to supply extra strength and stiffness to concrete section below crack.
- Epoxy interface between the concrete and CFRP plate.
- CFRP plate bonded to the concrete and extended above the concrete section to apply force.
- The only node that is fixed is the bottom of the M16 bolt.

All the elements have a size of 5x5 mm except at the crack position; no tension- and epoxy interfaces (Figure 41). A 3D experimental model layout with dimensions is given in Figure 17.

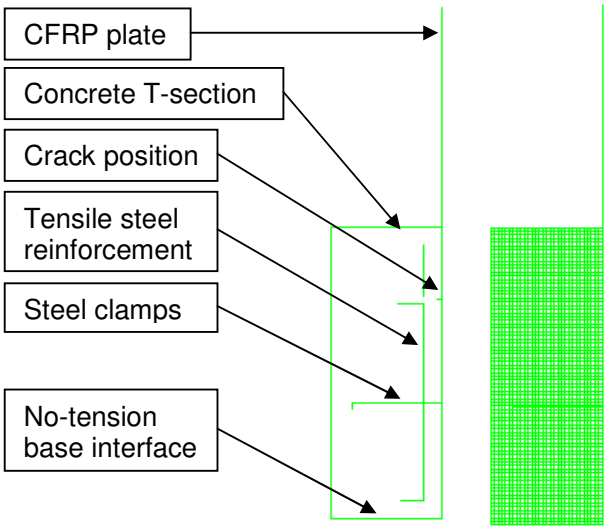


**Figure 41: T-Section analysis Layout**

Geometrical inputs for the model were:

Note: same notation for model layout as section 5.5.1.

| | | |
|---|---|---|
| Depth of all elements: | | 150mm, unless otherwise stated. |
| Concrete beam: | Width: | 150 mm |
| | Height: | 400 mm |
| | Depth of base: | 270 mm |
| Clamp plates: | Width: | 125 mm |
| | Height: | 8 mm |
| | Depth: | 80 mm |
| Reinforcement steel: | Area: | 314 $mm^2$ |
| | Length: | 250 mm |
| CFRP plate: | Area: | 70 $mm^2$ |
| | Length: | 600 mm |

The material input values were the same as for the beam analysis except for the concrete compressive strength as described in section 4.1.1.2.

### 5.7.2 Test 3 – Results

#### 5.7.2.1 Static loading

The analysis converged up to load step 42, the peak value in Figure 42. Step 43 was also converged, which is the point on the far right in Figure 42, although the full softening response has not been captured to confirm that the zero resistance is reached only at such a large displacement of roughly 0.8mm. The stress, rather than force, is plotted against the displacement because of the differences bond areas of the experimental tests. Stress in this instance is the applied force divided by the bonded area. This is a mere way of normalisation, and does not reflect uniform shear stress over the full height of the interface.

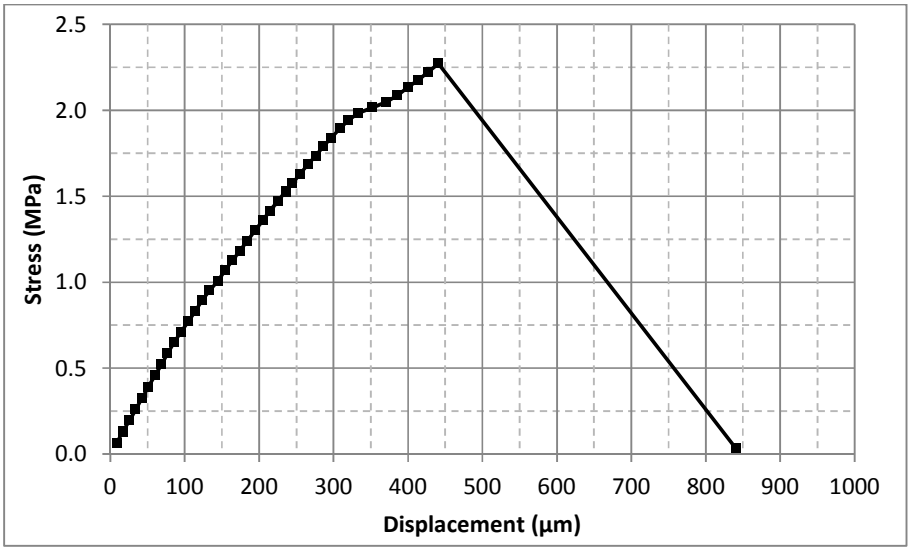


**Figure 42: Stress vs. Displacement of pull-off analysis**

At the peak force one can clearly see that the normal vertical stress (Figure 43) in the concrete is roughly equal to the stress at debonding of the CFRP plate which is an indication that the stress was transferred from the CFRP plate to the concrete. It is also clear that the maximum stress occurs around the crack in the model. From the outline of the structure in Figure 43 it seems that there is rotation of the specimen that indicate that there is a moment in the T-section which can be linked to a larger scale test of a simply supported beam as discussed in chapter 7.

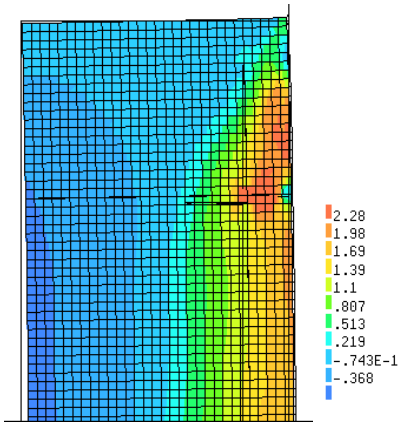


**Figure 43: Pull-off analysis: vertical normal stress result at peak resistance**

From the stress vs. displacement graph (Figure 42) and the normal stress distribution (Figure 43) of the analysis one can compare the local displacement for a more accurate comparison between the behaviour of the experimental tests and computational simulations.

The interface strain as defined in DIANA is the displacement of the CFRP plate relative to the concrete. For clarity it is referred to as relative displacement and will have a unit of mm. From Figure 44 it is visible that at the crack position there is a discontinuity in the relative displacement which is an indication that the crack has an influence on debonding.

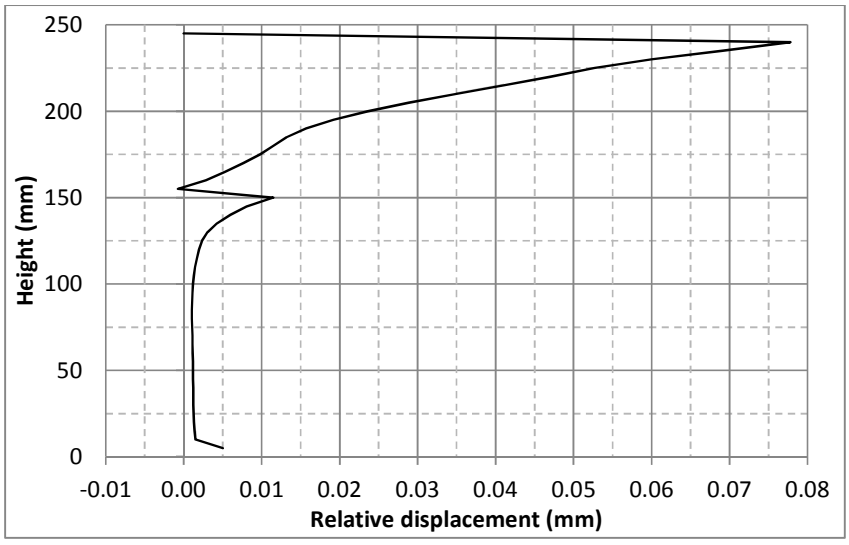


**Figure 44: DIANA Relative vertical (shearing) displacement between CFRP and concrete**

The generalised strain or relative shearing displacement presented in Figure 44 is the strain at 2 MPa, which is near the peak force and is representative of the relative displacement before debonding. The choice of the load step is discussed in section 4.5.

#### 5.7.2.2 Cyclic loading

##### 5.7.2.2.1 Cycles at 85% of pull-off force

The number of cycles reached in this analysis is 26. In Figure 45 one can see that the first few cycles displaced more than the subsequent cycles and at the end the growth in displacement increases until debonding, which is an indication that the model is a representation of real life beam response.

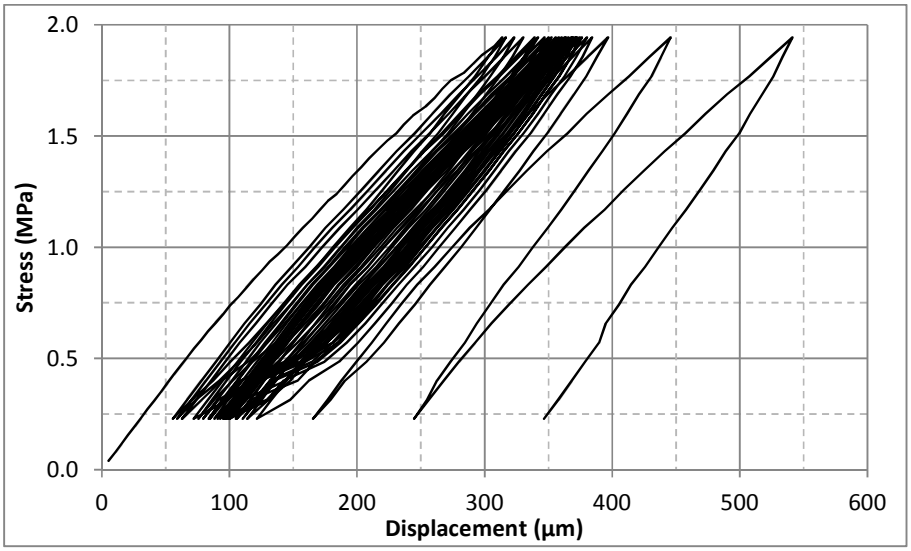


**Figure 45: Diana 85% Cycles**

In the fourth last cycle one can see that at the start of the cycle the displacement starts to deviate from the norm and that can be a result of the debonding that starts. The stress distribution of the T-Section at the 4$^{th}$ last cycle is given in Figure 46. It is clear that the vertical stress over the full length of the bonded interface is at or beyond the maximum bond stress, suggesting imminent plate debonding.

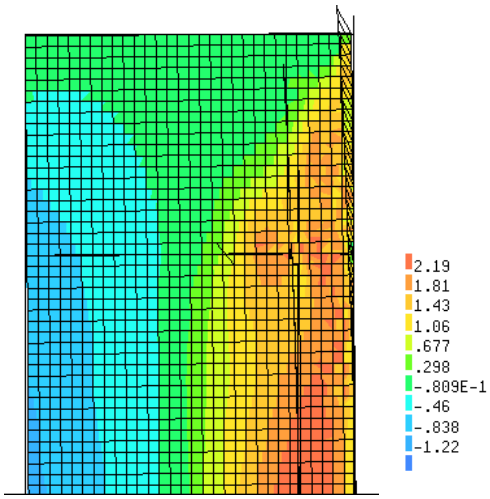


**Figure 46: 85% Cycles vertical normal stress distribution of 4th last cycle**

5.7.2.2.2 Cycles at 65% of pull-off force

The same setup was used for the 65% cycles as for the 85% and pull-off analyses, the difference is the amplitude of the force that was applied. The total number of cycles achieved was 196 before debonding of the CFRP plate. This is less than the number of cycles obtained from the experimental test, but it can be attributed to the difference in stiffness as explained in section 6.3.2.2.

As illustrated in Figure 47 the displacement growth per cycle is much less than for the 85% cycles and there is more cycles before the displacement starts to grow rapidly. The growth per cycle was very small suggesting that for cyclic loading at low force amplitude the fatigue behaviour of stress distribution is the same as static creep suggested by El-Tawil et al. (2001).

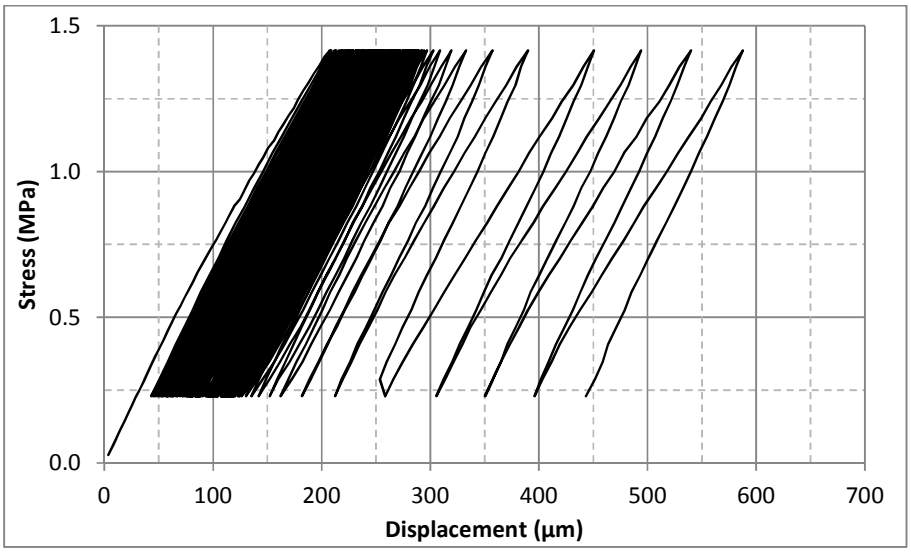


**Figure 47: Diana 65% Cycles**

Again a discontinuity is observed in the 5th last cycle. The cycles after that point can be ignored as explained in the next section about the failure envelope of the analysis.

Contrary to the experimental result (Section 4.5.1.2.2) of the local displacement observed by the Aramis system, the FE analysis show there is growth from cycle 5 to cycle 100 (Figure 48). This can be accounted to a difference in the stress range and the stiffness of the specimen, the concrete strength and interface thickness. Although the correct cube compressive strength of the concrete was used for the analysis the experimental T-section could have had a different strength due to difference in the compaction/vibration of the cubes and T-section.

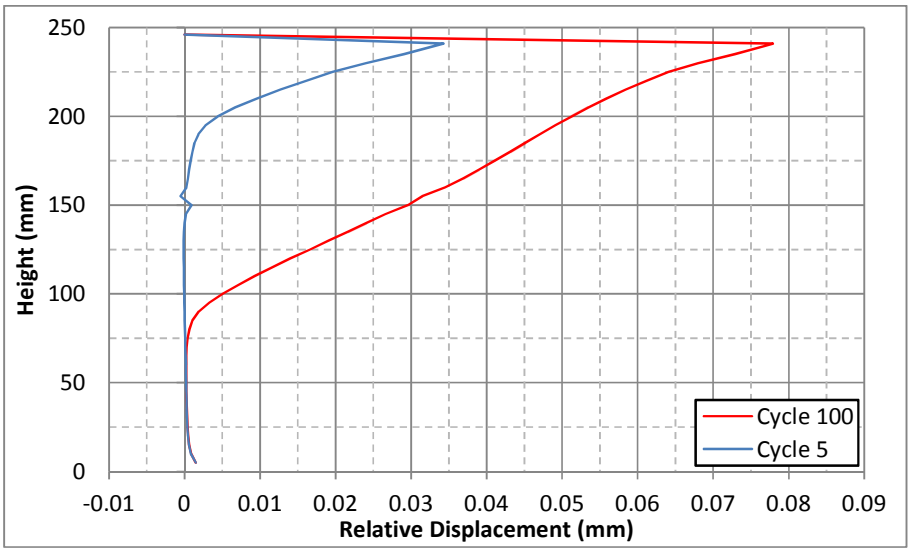


**Figure 48: Diana interface relative vertical (shearing) displacement (65% test)**

#### 5.7.2.3 Failure envelope

By plotting the three analyses on the same graph (Figure 49), it is clear that the stiffness in the first loading cycle for the cyclic tests is the same as the stiffness of the pull-off test. It is also apparent that both the stage II and stage III displacement growth per cycle is smaller for the 65% test than for the 85% test.

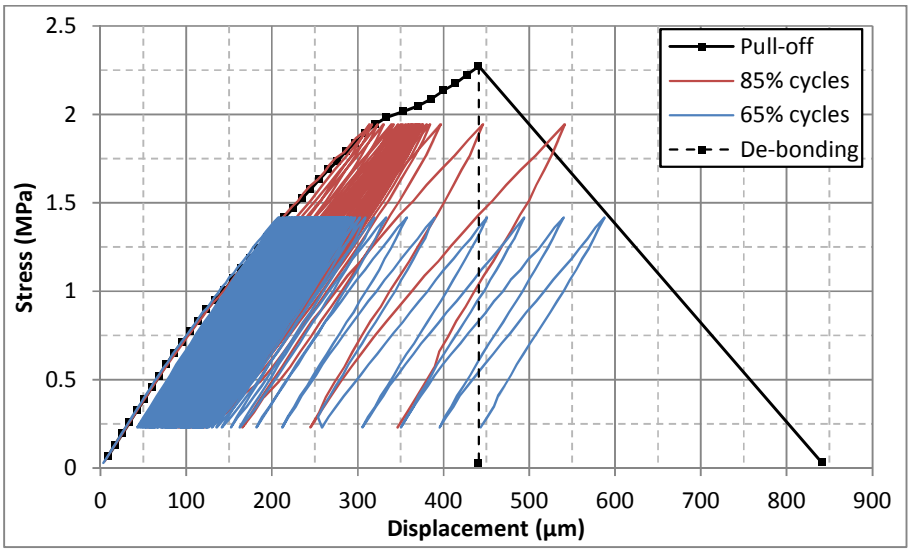


**Figure 49: Computed (DIANA) Failure envelope and cyclic responses of T- Section**

The debonding of the CFRP plate results in a rapid loss of resistance, thus at the peak stress of the pull-off analysis a line may be drawn vertically down. That would suggest that the last cycle of the 85% analysis and the last 4 cycles of the 65% analysis exceed the ultimate deformation that can be achieved under monotonic loading. Nevertheless, such large cyclic growths in the tertiary cyclic damage part (see Figure 45) are clearly beyond design consideration for practical application. The limit of the secondary (equal cyclic permanent displacement) part should be considered as an upper bound, which would suggest a snap-back in the pull-off envelope of this particular T-section specimen.

The 5$^{th}$ last cycle of the 65% analysis shows that at the bottom of the unloading there is a jump/discontinuity in the displacement that suggests the plate starts to debond and the last cycle of the 85% analysis can also be ignored because of the big step size at the maximum stress of the cycles.

# Chapter 6: Comparison of FEM and experiments

In this chapter the experimental results of chapter 4 are compared to the FE analyses of chapter 5.

## 6.1 Test 1 – Triplet Shear Tests

Plotted on the same graph (Figure 50) one can see that the results obtained from the experimental tests that were used for the analyses were accurate to the point of the first stress plato. The difference in stiffness can be explained by the boundary conditions. The roller supports used for the experiments is different from the no tension interface of the FE analyses.

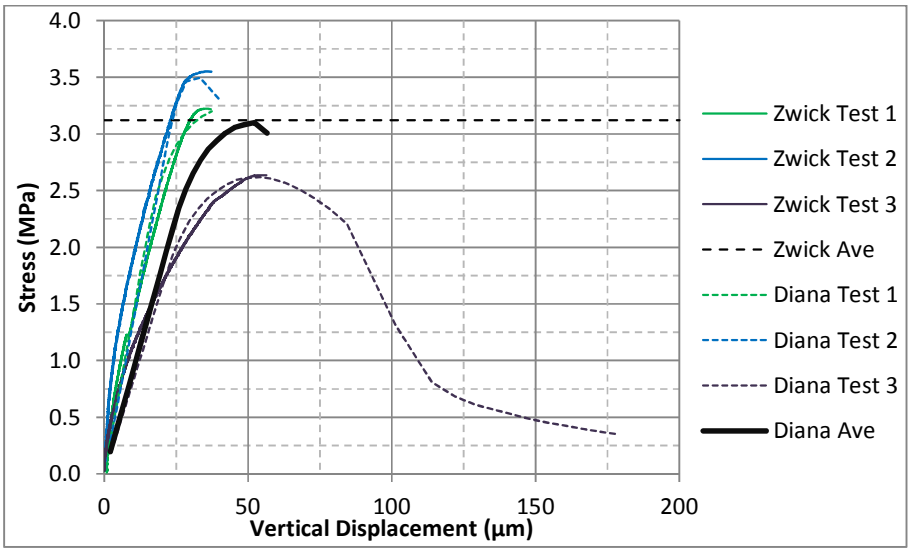


**Figure 50: Comparison of triplet results**

Because of the roller support used for the experimental tests it seems that the specimen rotated a bit resulting in a curved line for the initial stiffness that the FE analyses did not do.

## 6.2 Test 2 – Louw and Badenhorst Beam Analysis

As only the CFRP strengthened beam is considered the failure envelope of the experimental test by Louw (2009) can be ignored. It is only shown in Figure 51 to illustrate that the normal reinforced concrete (RC) beam still provides resistance. The analysis was stopped after debonding of the CFRP plate from the beam, because of the debonding of the plate the convergence criteria were not achieved and the solution became unreliable.

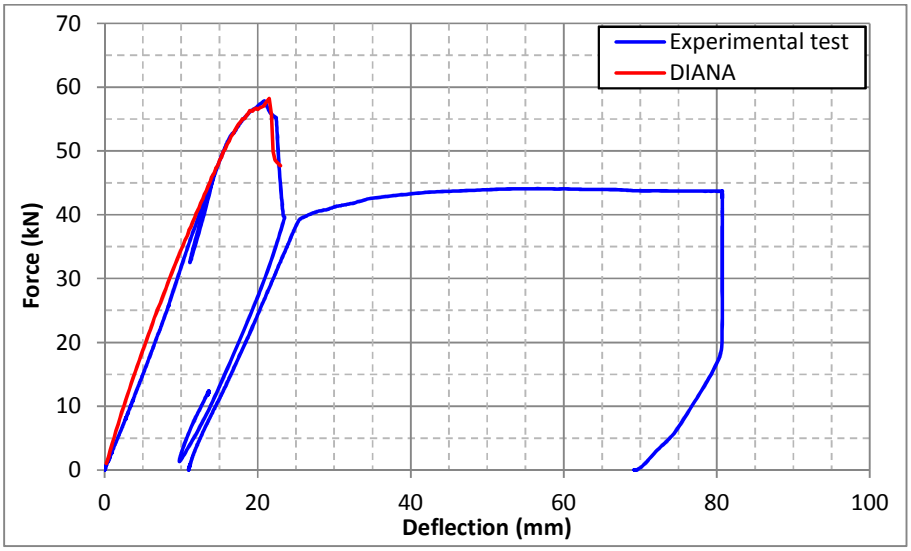


**Figure 51: Comparison of beam results**

The boundary conditions for the FE analysis and the experimental test where the same, a simply supported beam which is free to lift at the ends. At the supports a rubber pad was used for a more even stress distribution to the support. The loading plate size, beam dimensions, material properties and support conditions were the same for both cases, thus comparative stiffness and overall response was obtained from the FEA and the experiment.

This is a confirmation of the bond strength of the epoxy from test 1 (section 6.1) and can be used for the T-section.

## 6.3 Test 3 – Inverted T-Section

### 6.3.1 Static results

By comparing the static (pull-off) test of the T-section (Figure 52) it is observed that the peak stress (recall that this is a normalised representation of the T-section force deformational response) of the analysis is an average of the two experimental tests and the displacement is also in the same range as for the two tests.

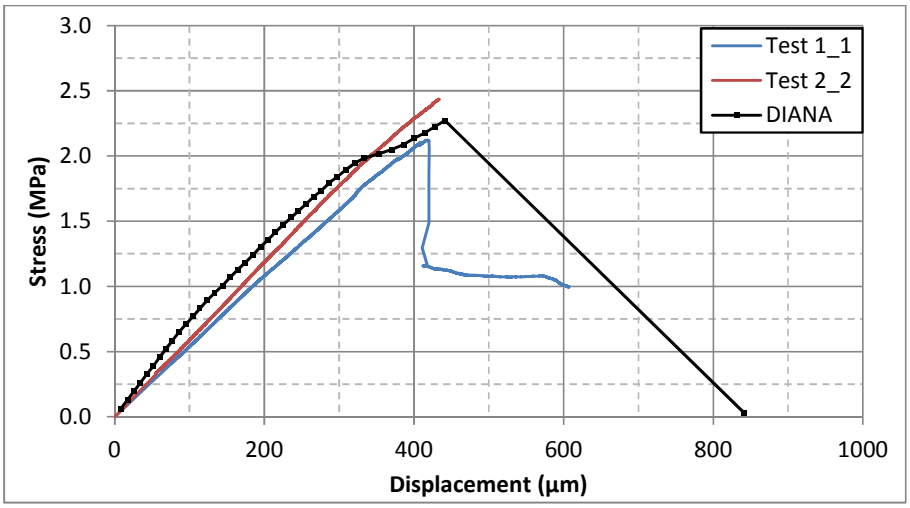


**Figure 52: Comparison of T-section pull-off tests**

By comparing the relative displacement of the FE results and the experimental test (Figure 53) at 2 MPa it can be confirmed that the FE analysis is similar to the experimental results and that for the design of the cyclic delamination model the calibrated FE analyses can be used. A maximum resolution of 10 µm in the particular test set-up complicates precise experimental characterisation of the delamination response.

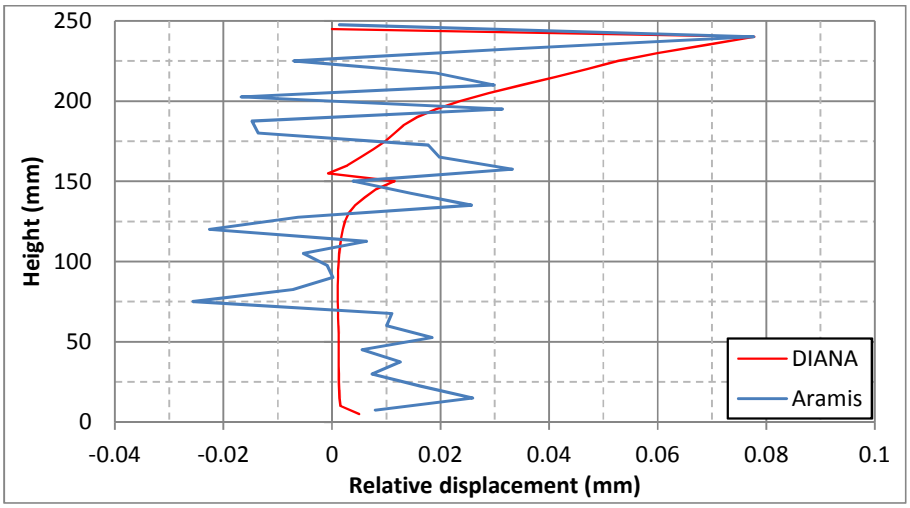


**Figure 53: Comparison of relative displacement for the pull-off tests**

### 6.3.2 Cyclic results

#### 6.3.2.1 85% Cycles

The initial stiffness of the experimental test and FE analysis differs, but the total displacement before debonding is comparable (Figure 54). Because of the bending of the CFRP plate in the experimental tests the displacement of the FE analysis will be used for comparison with the other results.

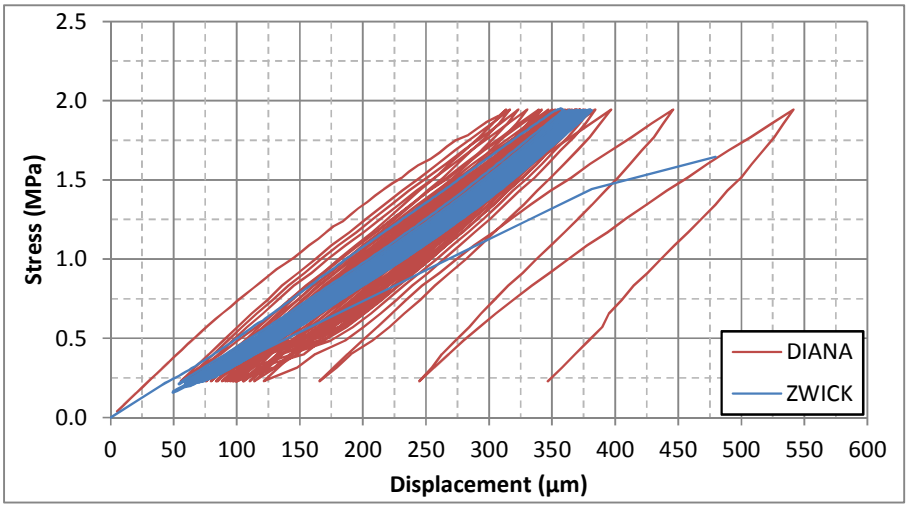


**Figure 54: Comparison of 85% cyclic tests**

The total displacement measured at the top of the concrete is compared to each other to verify the difference in stiffness of the experimental test and FE analysis (Figure 55).

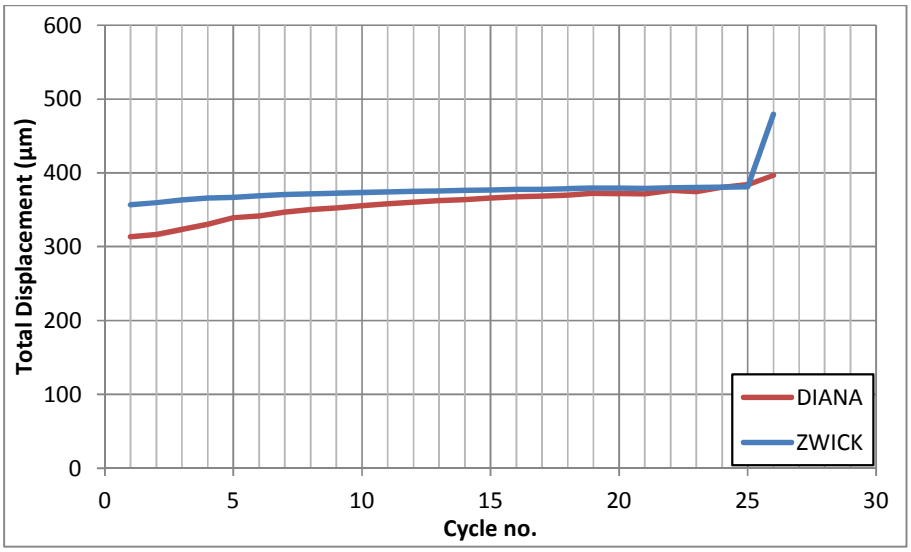


**Figure 55: 85% Cycles total displacement comparison**

The initial displacement difference is less than 50µm and from this comparison one can see that the displacement of the two tests is the same at the second last cycle indicating that the stiffness is the same.

#### 6.3.2.2 65% Cycles

For the cycles at 65% the total number of cycles differ (Experimental = 300 and FEA = 196). The reason for the difference in the number of cycles of the FEA and experimental test can be accounted to the concrete strength and the total bonding area of the CFRP plate on the concrete. The results are displayed on the same graph in Figure 56.

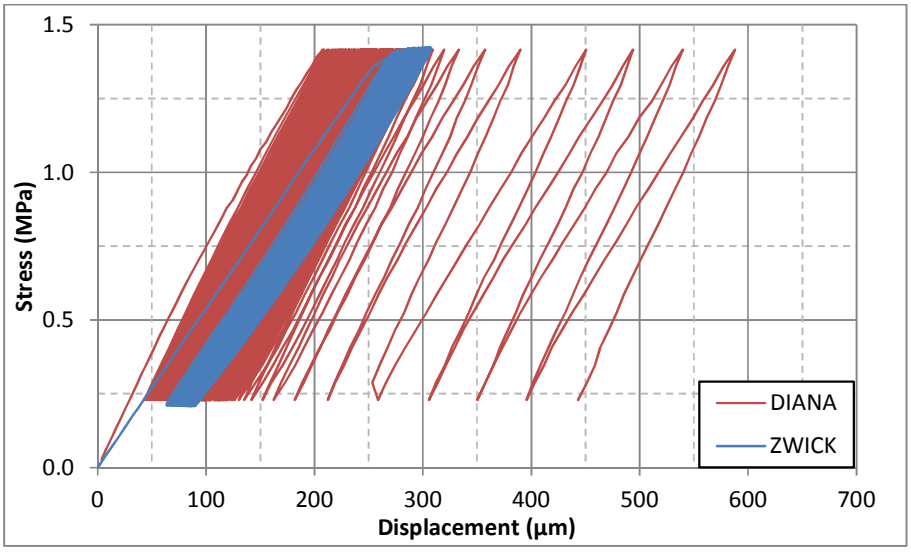

**Figure 56: Comparison of 65% cyclic tests**

The same graph was plotted for the 65% cyclic test (Figure 57) as for the 85% cyclic tests (Figure 55) and it is clear that the stiffness differs a lot (more than 50µm) for the experiment and the FEA.

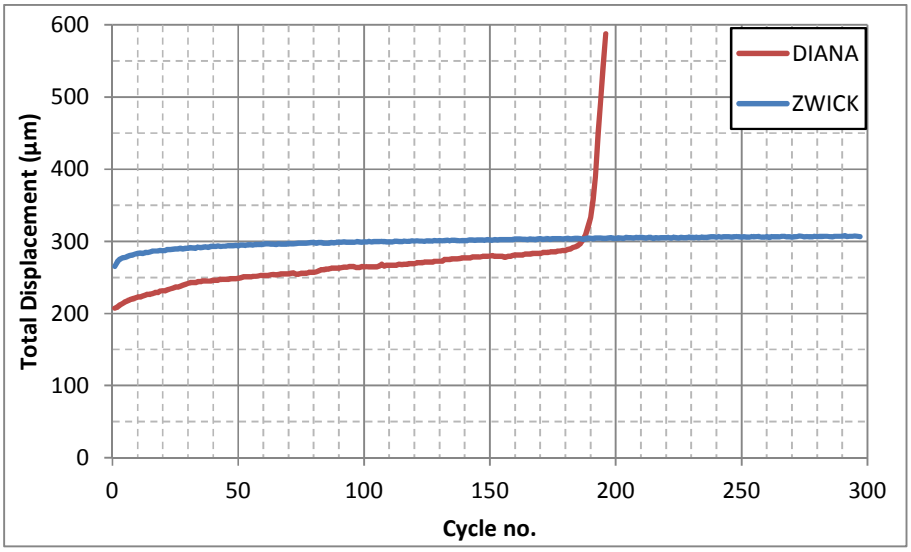


**Figure 57: 65% Cycles total displacement comparison**

For the T-section`s the analyses is deemed more reliable and it will be used for the model design.

# Chapter 7: Design model for cyclic debonding

For the design model for structures under cyclic loads it is necessary to link the designed test to a bridge beam and subsequently the number of cycles to the stress range it is subjected to. By normalising the relative displacement in the vicinity of a crack, by dividing it by the stress range the specific test was subjected to, one can quantify what the influence of the stress is for a certain force amplitude that the structure is designed for. The normalized relative displacement shown in log scale in Figure 58 suggests that there is a log-linear relationship between the number of cycles and the normalised relative displacement between stage II and stage III. Altought different input values were used for the concrete strength, the average compressive strength was taken to perform the analyses for 75%, 55% and 45% of the static pull-off stress. Due to the small variance in concrete strength of the experimental results used for the FE analyses, the results can be used for the model suggested below.

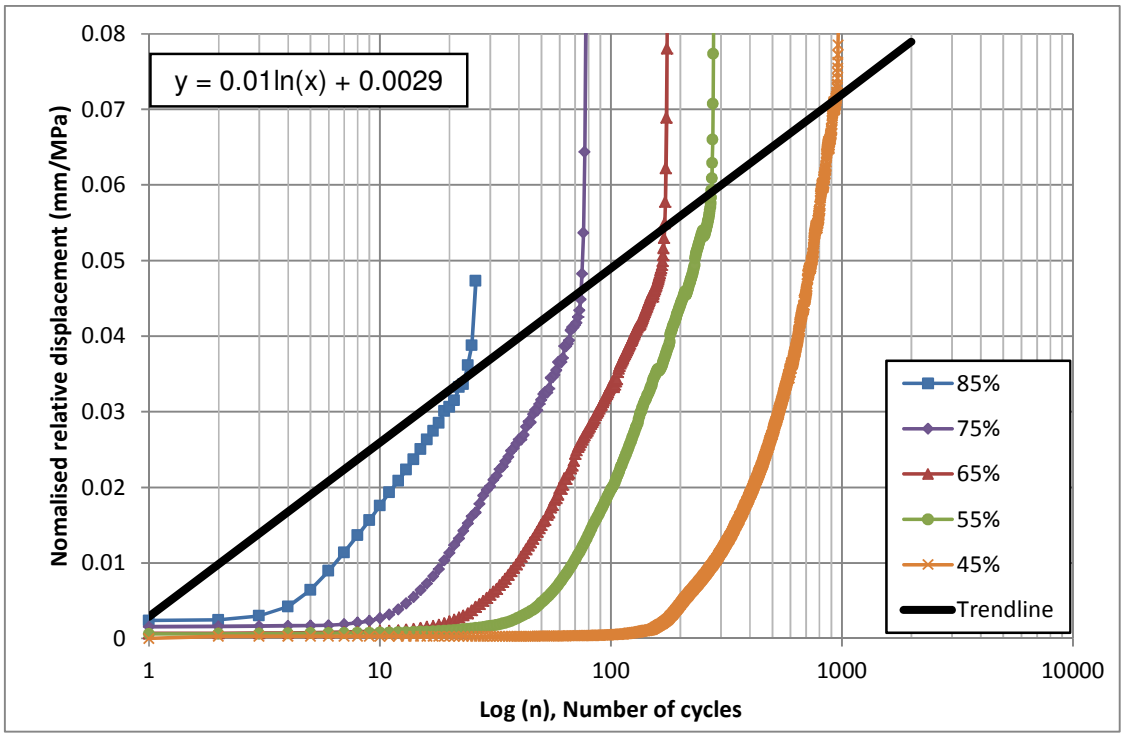


**Figure 58: Normalised relative displacement (Log scale)**

The straight line in Figure 58 is a suggestion of the maximum allowable normalized relative displacement in the vicinity of a crack. Although only the 85% and 65% cyclic FE analyses were compared to experimental tests, 75%, 55% and 45% analyses were done for confirmation of the line. After the suggested number of cycles the structure is in stage III of

the displacement and thus suggests that total delamination of the CFRP plate will occur rapidly (within a few cycles) after that point. It is also apparent that for the 75% and 85% cyclic tests the initial relative displacement is larger than for the 65%, 55% and 45% tests. This suggests that the serviceability cyclic loading on a structure (67%) will not have a significant effect on the design, but cyclic loading at a force amplitude larger than that can cause damage more rapidly.

When the same results are plotted on a linear scale non-linearity`s starts to appear (Figure 59). When the normalised relative displacement exceeds 0.065mm/MPa the relationship between it and the number of cycles for the 45% cyclic analysis starts to step which can be attributed to the transition from stage II to stage III before debonding thus the limit must be before the transition.

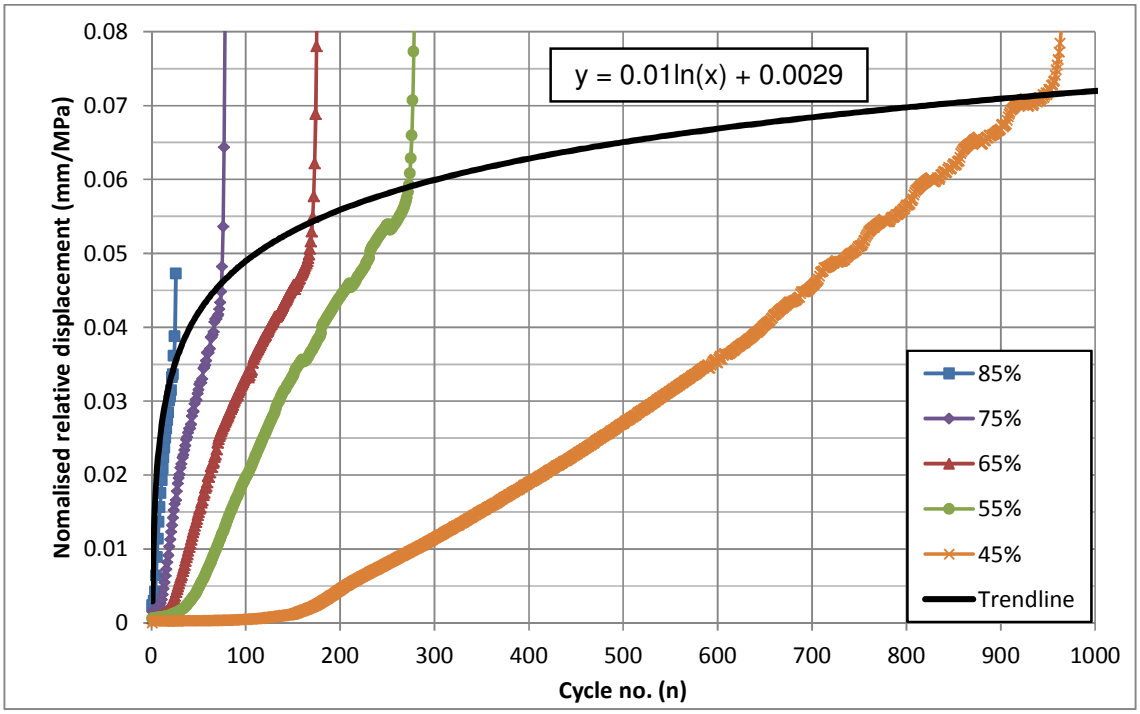


**Figure 59: Normalised relative displacement (Linear scale)**

The trend line through the results indicate that the limit for normalised relative displacement between the CFRP plate and the concrete in the vicinity of a crack for stage II has a limit of 0.065mm/MPa for the 45% analysis and by optimizing the initial slope of the graph also suggests that the 85% cyclic test is an outlier and that cyclic loading for that stress range should not be considered due to the low number of cycles that can actually be achieved.

The proposed equation for the limit of normalised relative displacement is:

$$NRD = 0.01\ln(n) + 0.0029 \qquad \text{eq. 1}$$

For eq. 1, NRD is the Normalised Relative Displacement and n is the number of cycles. The number of cycles can be limited by and linked to the stress range and force amplitude at which cyclic loading is done.

From Figure 59 it seems that there is no initial delamination (plastic relative displacement or permanent displacement/damage) of the CFRP plate until a certain threshold number of cycles for low load amplitudes. By subtracting the elastic relative displacement ($-\sigma/K_s$) from each analysis one can see that for the 75% and 85% analyses there is no threshold and that delamination starts from the first cycle, but for the other 3 analyses the delamination initiation threshold is indicated in Figure 60. From there the delamination initiates at a low but increasing rate until a constant rate of delamination is observed. The stress ($\sigma$) used to determine the elastic relative displacement was the respective stress of the stress range of each analysis.

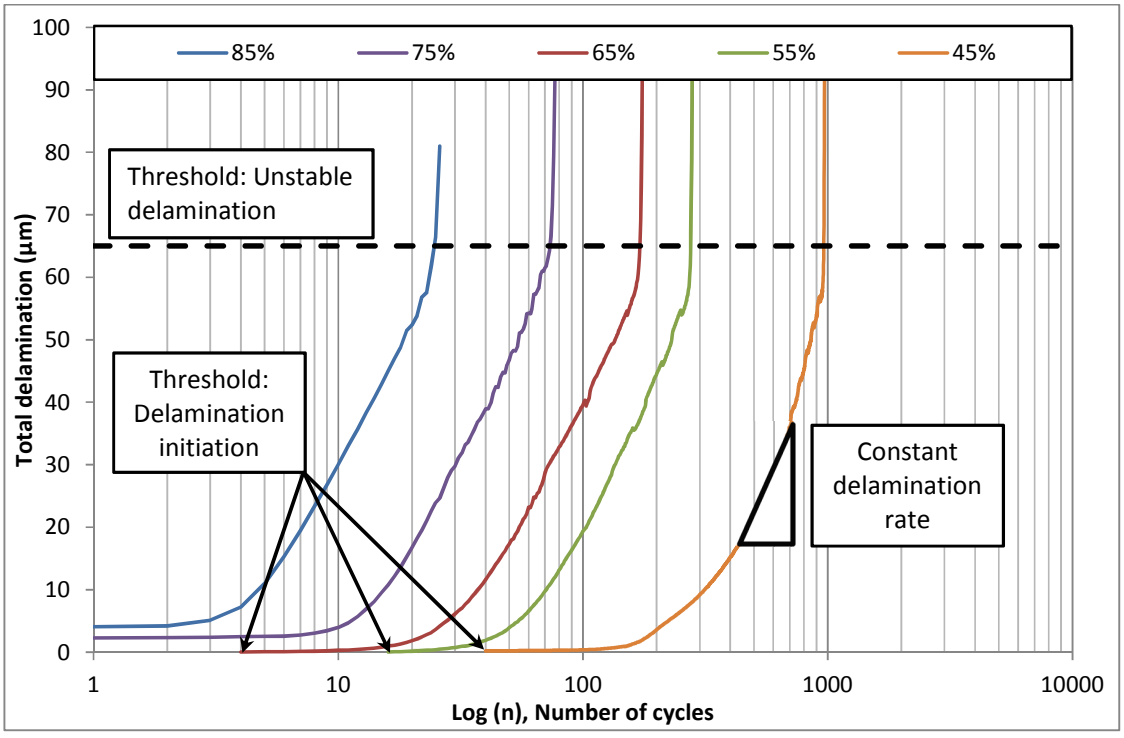


**Figure 60: Total plastic relative displacement**

The latter constant delamination rate is significantly lower for a lower cyclic force amplitude, i.e. for the 45% cyclic analysis the mination rate (growth rate of delamination) is smaller than the rate of the 55% analysis. As seen in Figure 60 the 45% cyclic analysis almost reaches 1000 cycles before it nears the 65 µm line where the unstable delamination rate starts, and the 55% analysis almost reach 200 cycles. The unstable delamination threshold is at a delamination level of about 65 µm for all cases (Figure 60).

In Figure 61 the delamination initiation and unstable delamination threshold is shown and it suggests that for the unstable threshold there can be a limit at which point the CFRP plate will not delaminate from the RC structure.

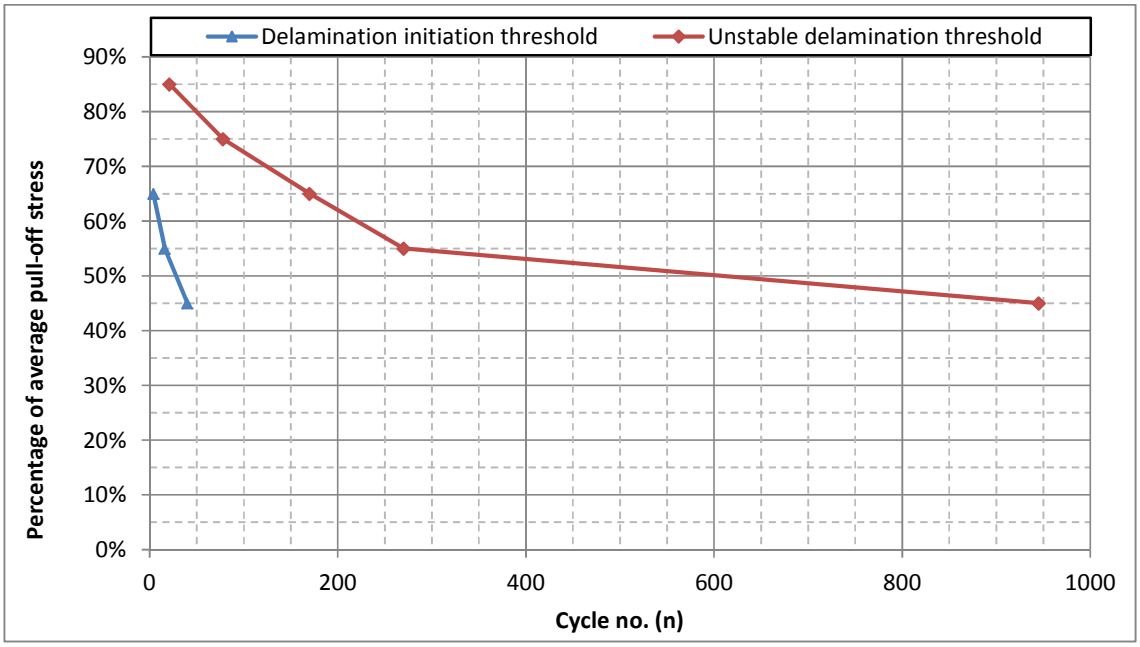


**Figure 61: Delamination Thresholds**

The existence of a fatigue limit would require that, for an appropriately low load cycle level, an infinite delamination initiation limit exists which means that delamination does not start. Alternatively for a sufficiently large number of load cycles, equating to a particular service life, the fatigue life design would require that an appropriately low delamination rate is realised so that the threshold delamination level leading to unstable delamination and complete pull-off of the CFRP plate is not realised before the design number of cycles.

It must be noted that the link from delamination rates in the T-section to full scale beam bending must be made in order to scale the number of load cycles appropriately. Such

linking must consider crack formation, crack proximity (spacing) and delamination caused at several cracks by a single passing wheel load. This falls beyond the current Master's thesis, but is the subject of the continued research group. Nevertheless, significant insight has been developed in cyclic delamination of CFRP plates from a standard concrete class in the South African context.

For the translation of the T-section results to a CFRP strengthened RC beam, careful analysis of the stress transfer is required. It is argued that, in the uncracked beam, horizontal shear stress in the bond between the CFRP plate and the concrete is caused by a varying bending moment along the length of the beam. This may lead to crack formation under service loads. Subsequently, shear stress in the interface may be dominated by transferring the moment-induced tensile force in the CFRP plate at the cracked cross-section to the concrete at uncracked cross-sections. This latter shear transfer mechanism is similar to the situation in the T-section. It must however be kept in mind that an overall axial tensile force accompanies the bending moment in the T-section, while the axial force or axial stress resultant in a beam is usually zero. Thus, the shear transfer in the T-section may be more severe that in a beam, which remains to be studied in detail. For this further research, the calibrated FE model and model parameters for this particular materials used in this research, will be of key value.

# Chapter 8: Conclusion

This thesis focussed on the debonding of CFRP plates from concrete structures under cyclic loading, specifically the delamination of the plates in the vicinity of a single crack. The following conclusions can be made from the study:

1. Debonding of CFRP plates from a single concrete class (35 MPa cube compressive strength) was studied and successfully simulated numerically. This was done in Triplet tests to study the near pure shear response along an epoxy-bonded joint which dominantly fails in the concrete substrate. It was also confirmed in a specially designed RC T-section.

2. The characterised bond model parameters were used in the FE analysis of a RC beam strengthened with a CFRP plate, leading to accurate simulation of observed and captured response of a physical experiment. All sources of nonlinearity, including the interfacial bond between concrete and CFRP, uplift at the far end of bearing supports and crack formation in the concrete substrate were simulated, leading to good global agreement with the observed response.

3. Having verified the agreement between FE models and experimental observations in two quasi-static monotonic loading experimental setups, cyclic loading was analysed and compared with cyclic debonding experiments in the designed RC T-section. Reasonable agreement in peak resistance for the monotonic case was achieved. For the cycles at 85% of the peak stress the same number of cycles to failure was observed for both the FE analysis and the experiment, but a difference in the number of cycles to failure at 65% of the peak stress cyclic load was found. Nevertheless, the cyclic growth in delamination was considered to be well captured in the FE analyses, and used for characterisation of growth in delamination under cyclic loading of several more stress amplitudes (45%, 55% and 75% cyclic analyses).

4. From the analyses of the cracked RC T-section the delamination (relative displacement between the CFRP plate and concrete substrate) in the vicinity of a crack was then used to determine the threshold for:
   a. Initiation of delamination: the number of cycles to such initiation is not constant, but increases with reduced load level. For the 85% and 75% cases delamination started from the first step. For all the cases analysed below and including 75% of the pull-off load, delamination initiated after an increased number of cycles with reduced stress level. It remains to be shown whether a threshold shear stress level may exist below which delamination will not initiate irrespective of the number of load cycles.
   b. Unstable delamination (onset of phase III): At that point the rate of delamination is rapid until the CFRP plate has completely debonded from the RC T-section. It appears that this occurs at a delamination level of 55-65μm in all cases investigated. This may have been influenced by the delamination growing from the top of the T-section specimen and remains to be verified through FEA of a specimen with a larger distance to the crack in the RC.

Although a small data basis of tests was done, the variety of analyses with reasonable confirmation of experimental tests goes a long way to confirm the experimental results.

Future research that need to be done include:

- Testing of larger scale beams in flexure with multiple cracks, hereby linking the designed T-section tests with actual cycles in beams that can determine debonding. It can further be verified whether a fatigue limit exists for cyclic debonding of CFRP plates from a cracked beam, as opposed to none found for the T-section computationally in this work for a load level as low as 45% of peak resistance.

- Different strength concrete and its bonding properties as well as the type of cement used for the concrete mixes. Hereby the design recommendations can be generalised to more concrete strength classes, where for instance delamination occurs along the CFRP plate and not in the concrete substrate in cases of high strength concrete.

- Generalisation of the results will require inclusion of also shear-dominated cracking, which may lead to larger delamination per loading than bending crack-induced delamination.

- This study also only investigated epoxy and CFRP plates from one supplier, the bond strength of other epoxies also need to be tested under cyclic loading to get confirmation thereof.

- The influence of the crack position from the top of the RC T-section also need to be determined to determine what the effective bond length of the epoxy is under cyclic loading.

# Chapter 9: Bibliography


1. ACI 318-95. (1999). *Building Code Requirements for Structural Concrete (318-95) and Commentary (318R-95).* Michigan, USA: American Concrete Institute (ACI).
2. Aidoo, J., Harries, K. A., & Petrou, M. F. (2002). *Fatigue behaviour of CFRP-Strengthened reinforced concrete bridge girders.* Columbia, SC: University of South Carolina.
3. Al-Hammoud, R., Soudki, K., & Topper, T. H. (2011). Fatigue flexural behaviour of corroded reinforced concrete beams repaired with CFRP sheets. *ASCE Journal of Composites for Construction* , 42-51.
4. Badenhorst, A. J. (2009). *KVVP Plakbewapening vir brugversterking.* Stellenbosch University, Stellenbosch.
5. Barnes, A., & Mays, G. C. (1999). Fatigue performance of concrete beams strengthened with CFRP plates. *ASCE Journal of composites for construction, Vol. 3 No. 2* , 63-72.
6. Bazant, Z., & Oh. (1983). Crack band theory for fracture of concrete. In *Materials and Structures* (pp. 155-177).
7. British Standards Institute (BSI). (2002). *EN 1990 - Basis of structural design.* London: British Standards Institute (BSI).
8. British Standards Institute (BSI). (2004). *Eurocode 2: Design of concrete structures.* London: British Standards Institute (BSI).
9. Buyukozturk O, G. O. (2003). Progress on understanding de-bonding problems in reinforced concrete and stell members strengthened using FRP composites. *Construction and Building Materials* , 18:9-19.
10. DIANA, 9. E. DIANA Element Library, Part 1. In *Structural Analyses.* Delft, The Netherlands: TNO DIANA.
11. DIANA, 9. M. DIANA Material Library, Part 1. In *Structural Analysis.* Delft, The Neterlands: TNO DIANA.
12. El-Tawil, S., Ogunc, C., Okeil, A., & Shahawy, M. (2001). Static and fatigue analyses of RC beams trengthened with CFRP laminates. *Journal of composites for construction* , 258-266.
13. Gravina, R., & Smith, S. (2005). Critical de-bonding length in FRP flexurally strengthened RC members. *International Symposium on Bond Behaviour of FRP in Structures.*
14. Jiang JJ, L. X. (2004). *Bond-Slip models for FRP sheet/plate-to-concrete interfaces.* Woodhead Publishing Limited.

15. Louw, J. (2009). *The effect of cyclic loading on CFRP strengthened beams.* Stellenbosch University, Stellenbosch.
16. *Mapei South Africa (Pty) Ltd*. (n.d.). Retrieved from http://www.mapei.co.za
17. Smith ST, Teng JG. (2002). FRP-Strengthened RCbeams. I: Review of de-bonding strength models. *Engineering Structures 24* , 385-395.
18. Teng, J., Chen, J., Smith, S., & Lam, L. (2002). *FRP Strengthened RC Structures.* Chichester, West Sussex, England: John Wiley & Sons, Ltd.

# Appendix A: Concrete Mix design

The same concrete mix was used for this study as for the final year project of Badenhorst (2009). The mix had to be adjusted because of the different batches of cement received. The Surebuild cement properties are also listed in Table A1 to compare to the chosen designed OPC mix.

**Table A1: Concrete mix design**

| | Material | FM | CBD (kg/m$^3$) | RD |
|---|---|---|---|---|
| Cement | OPC 42.5 | | 1500 | 3.14 |
| | Surebuild 32.5 | | 1500 | 3.04 |
| Sand | Philippe | 1.5 | | 2.69 |
| | Crusher dust | 3.6 | | 2.71 |
| | Malmesbury | 2.3 | | 2.60 |
| Aggregate | 6 mm | | 1535 | 2.70 |
| | 13 mm | | 1495 | 2.70 |
| | 19 mm | | 1577 | 2.72 |

| | | OPC | Surebuild | |
|---|---|---|---|---|
| **W/C ratio** | | | | |
| | Addis (1998) p. 108 | 0.6 | 0.53 | |
| **Water required** | | | | |
| | 6mm Aggregate | 195.0 | 202.5 | kg |
| | minus 20 % | 195.0 | 202.5 | liter |
| **Sement content** | | | | |
| | C = W/(W/C) | 325.00 | 382.01 | kg |
| | | 103.50 | 125.66 | liter |
| **Aggregate content** | | | | |
| | St = CBDst(K-0.1FM) | 1061.45 | 1089.85 | kg |
| Addis p. 110 | K = 0.94 | 393.13 | 403.65 | liter |
| | Malmesbury sand | | | |
| **Sand content** | | 801.75 | 697.38 | kg |
| | | 308.37 | 268.22 | liter |
| | Total | 1000.00 | 1000.00 | liter |
| | Total | 2383.20 | 2371.71 | kg |

Justification of chosen materials:

- OPC cement – Better bond of epoxy and concrete. (Discussed in Section 3.1)
- 6mm aggregate – Small specimens to increase compaction and workability.
- Malmesbury sand – Better quality sand in comparison to Philippi.

The average slump obtained from the concrete mixes was 100mm, which was sufficient due to the narrow spacing of the reinforcement steel and workability.

No admixtures or fibres were used in the mix.

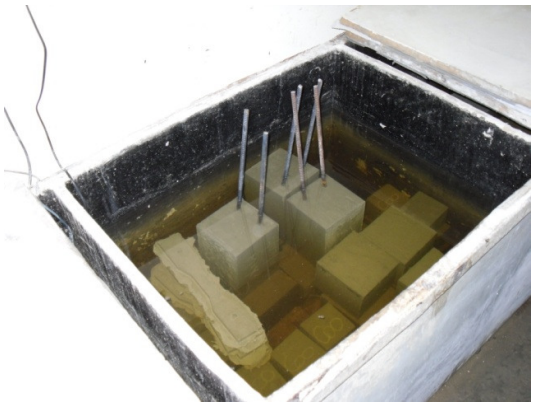

All the concrete specimens was cured in water with a constant temperature for 7 days, there after the specimens were removed to dry before the CFRP plates was applied.

# Appendix B: Computational input

## Triplet computational input

```
MATERIALS
: CONCRETE
/ 211-390 / 1
: Epoxy interface
/ 181-210 453-478 / 2
: Steel
/ 1-150 481-654 / 3
: NO TENSION INTERFACE
/ 655-664 / 5
GEOMETRY
: Epoxy interface 55%
/ 453-478 / 1
: Epoxy interface full
/ 181-210 / 2
: Concrete
/ 211-390 / 3
: Steel
/ 1-150 481-654 / 4
: No tension interface
/ 655-664 / 5
'MATERIALS'
  1 YOUNG 2.41E+04
    POISON 2.50E-01
  2 dstif 1.1E+2 0.65E+2
    COMBIF
    GAPVAL 3.105
    MO1VAL 0.0452
    FRCVAL 3.105 1.0 0.001
    MO2VAL 0.35
CAPVAL 37. 0.9
MOCVAL 100. 0.1
  3 YOUNG  210.E+03
    POISON 2.0E-01
: NO TENSION INTERFACE
  5 dstif  1.0e+10 0.1e+0
'GEOMETRY'
: Epoxy interface 80%
  1 THICK     11.000000E+01
    CONFIG MEMBRA
: Epoxy interface full
  2 THICK     15.000000E+01
    CONFIG MEMBRA
:  Concrete
  3 THICK     1.500000E+02
:  Steel
  4 THICK     15.00E+01
: NO TENSION INTERFACE
  5 THICK     1.500000E+02
    CONFIG MEMBRA
'TYINGS'
EQUAL TR 2
  435 404
  466 404
  497 404
  528 404
  559 404
  611 614
  612 614
  613 614
  615 614
  616 614
  617 614
'SUPPORTS'
: / 1 32 63 94 125 156 / TR 1
 / 1 32 63 94 125 156 / TR 2
: / 1 32 63 94 125 156 / TR 3
 / 614 / TR 1
 / 614 / TR 2
: / 614 / TR 3
: / 404 / TR 1
 / 404 / TR 2
: / 404 / TR 3
'LOADS'
CASE 1
Nodal
DEFORM
  614              TR              2              -5
```

## Beam computational input

```
MATERIALS
:CONCRETE
/ 1-2400 / 1
:CFRP BEAM
/ 2537-2672 / 2
:EPOXY INTERFACE
/ 2401-2536 / 3
:RUBBER
/ 4000-4019 / 10
:STEEL TOP
/ 4020-4029 / 6
:NO TENSION INTERFACE
/ 5000-5019 / 7
GEOMETRY
:BEAM
/ 2537-2672 / 1
:concretetop
/ 1-2400 / 2
: EPOXY INTERFACE
/ 2401-2536 / 3
:RUBBER
/ 4000-4019 / 10
:STEEL TOP
/ 4020-4029 / 7
:NO TENSION INTERFACE
/ 5000-5019 / 8
'MATERIALS'
  1 YOUNG     2.41E+04
    POISON    2.0E-01
    TOTCRK ROTATE
    TENCRV HORDYK
    TENSTR 3.37
    GF1    0.1
COMCRV  MULTLN
COMPAR    0.0  0.0  -9.75  -0.0001086  -19.62
                -0.000293   -35.51   -0.0007813   -
37.45
-0.000917 -39.47 -0.0014081 -37.44
-0.001911 -33.97 -0.0025801 -32.42
       -0.002630 -30.98 -0.0027
:::::::::::::: CFRP BEAMS::::::::::::::::::
  2 YOUNG     200.0000E+03
    POISON    1.000000E-02
:::::::::::::: EPOXY INTERFACE ::::::::::::::
  3 dstif 1.1E+2 0.65E+2
    COMBIF
    GAPVAL 3.105
    MO1VAL 0.0452
    FRCVAL 3.105 1.0 0.001
    MO2VAL 0.35
CAPVAL 37. 0.9
MOCVAL 100. 0.1
::::::::::::::REBAR STEEL ::::::::::::::::::
4 YOUNG     206000.
    POISON    2.500000E-01
    YIELD VMISES
    HARDEN WORK
HARDIA 550. 0. 640. 0.09
:::::::::::::: STAAL TOP ::::::::::::::::::
  6 YOUNG     2.100000E+05
    POISON    1.500000E-01
:::::::::::::: NO TENSION INTERFACE ::::::
  7 dstif  1.0e+10 0.1e+0
:RUBBER
  10 YOUNG    5.000000E+01
    POISON    4.500000E-01
'GEOMETRY'
:BEAM
  1 CROSSE    7.000000E+01
    INERTI    1.458333E+04
:Conctop
  2 THICK     1.500000E+02
:epoxy interface
  3 THICK     5.000000E+01
    CONFIG MEMBRA
:REBAR
```

```
4 CROSSE    314.
5 CROSSE    10.
9 CROSSE    236.
:STEEL TOP
  7 THICK     1.500000E+02
:::::::::::::: NO TENSION INTERFACE :::::
  8 THICK     1.500000E+02
    CONFIG MEMBRA

:::::::::::::: RUBBER ::::::::::::::::::
  10 THICK     1.500000E+02
'REINFO'
LOCATI
  3000 BAR
LINE  3000 3003
  3001 BAR
LINE  3001 3002
  3003 BAR
      LINE 3006 3001
      LINE 3002 3007
MATERI
 / 3000-3001 3003 / 4
GEOMET
3000  4
3001  5
3003  9
'TYINGS'
EQUAL TR 2
4000 4005
4001 4005
4002 4005
4003 4005
4004 4005
4006 4005
4007 4005
4008 4005
4009 4005
4010 4005
4011 4016
4012 4016
4013 4016
4014 4016
4015 4016
4017 4016
4018 4016
4019 4016
4020 4016
4021 4016
4022 4027
4023 4027
4024 4027
4025 4027
4026 4027
4028 4027
4029 4027
4030 4027
4031 4027
4032 4027
'SUPPORTS'
:/ 6 156 / TR 2
/ 4005 / TR 2
/ 4016 / TR 2
/ 4027 / TR 1
/ 4027 / TR 2
:/ 11 151 / TR 2
'LOADS'
CASE 1
DEFORM
  4027 TR 2 -25
```

## T-Section computational input

```
MATERIALS
:CONCRETE
/ 1-1800 1831-2430 1801-1830 /  1
:CFRP BEAM
/ 2471-2511 2542 2560-2569 2600-2613 /  2
:crack interface
:/ 1801-1830 /  3
:epoxy interface
/ 2431-2470 2550-2559 /  4
:steel screws + CLAMP
/ 2512-2541 2700-2724 /  5
:base interface
/ 2725-2754 /  6
GEOMETRY
:BEAM
/ 2471-2511 2542 2560-2569 2600-2613 /   1
:conctop
/ 901-1800 1831-2430 1801-1830 / 2
:epoxy interface
/ 2431-2470 2550-2559 /  4
:concbot
/ 1-900 /  5
:steel screws
/ 2512-2541  /  6
:base interface
 / 2725-2754 /  7
:CLAMP
/ 2700-2724 / 10
'MATERIALS'
   1 YOUNG     28253.42567
     POISON    2.000000E-01
     TOTCRK ROTATE
     TENCRV HORDYK
     TENSTR 2.57105
     GF1     0.1
COMCRV  MULTLN
COMPAR  0.0 0.0 -7.59069 -0.00011 -16.2669
        -0.00029 -28.6326 -0.00078 -30.1366
        -0.00092 -33.7105 -0.00141 -31.1314
        -0.00191 -27.4334 -0.00258 -26.2236
        -0.00263 -24.1048 -0.00265

:::::::::::::: CFRP BEAMS::::::::::::::::::
   2 YOUNG     200.0000E+03
     POISON    1.000000E-02
:::::::::::::: EPOXY INTERFACE ::::::::::::::
   4 dstif 1.1E+2 0.65E+2
     COMBIF
     GAPVAL 3.105
     MO1VAL 0.0452
     FRCVAL 3.105 1.0 0.001
     MO2VAL 0.35
CAPVAL 37. 0.9
MOCVAL 100. 0.1
   5 YOUNG     2.060000E+05
     POISON    1.500000E-01
   6 dstif  1.0e+10 0.1e+0
::::::::::::REBAR STEEL ::::::::::::::::
7 YOUNG     206000.
     POISON    2.500000E-01
     YIELD VMISES
     HARDEN WORK
HARDIA 550. 0. 640. 0.09
'GEOMETRY'
:BEAM
   1 CROSSE    7.000000E+01
     INERTI    1.458333E+04
:Conctop
   2 THICK     1.500000E+02
:epoxy interface
   4 THICK     5.000000E+01
     CONFIG MEMBRA
:Concbot
   5 THICK     2.900000E+02
:steel screw
   6 CROSSE    402.12
```

```
INERTI    6434.
:base interface
   7 THICK     2.900000E+02
     CONFIG MEMBRA
:REBAR
8 CROSSE    314.
9 CROSSE    157.

:CLAMP
   10 THICK    8.00E+01
'REINFO'
LOCATI
   3000 BAR
LINE  181 1855
   3001 BAR
LINE  175 181
LINE  1948 2382
LINE  1848 1855
MATERI
 / 3000-3001 / 7



GEOMET
3000  8
3001  9
'SUPPORTS'
 / 2585-2615 / TR 1
 / 2585-2615 / TR 2
 / 2585-2615 / TR 3
 / 2641 / TR 1
 / 2584 / TR 1
 / 2584 / TR 2
 / 2583 2627-2640 2616 / TR 1
'LOADS'
CASE 1
DEFORM
2584 TR 2 2.
```

This input is for the Pull-off analysis of the T-Section, by changing the load control from displacement to force for the cyclic tests the input will change to:

```
85% Cycles
CASE 1
Nodal
   2584 Force    2    24278.125
CASE 2
Nodal
   2584 Force    2    21421.875

65% Cycles
CASE 1
Nodal
   2584 Force    2    17723.47077
CASE 2
Nodal
   2584 Force    2    14867.22077
```